Molecular Cell

Article

Noncanonical mono(ADP-ribosyl)ation of zinc finger SZF proteins counteracts ubiquitination for protein homeostasis in plant immunity

Graphical abstract

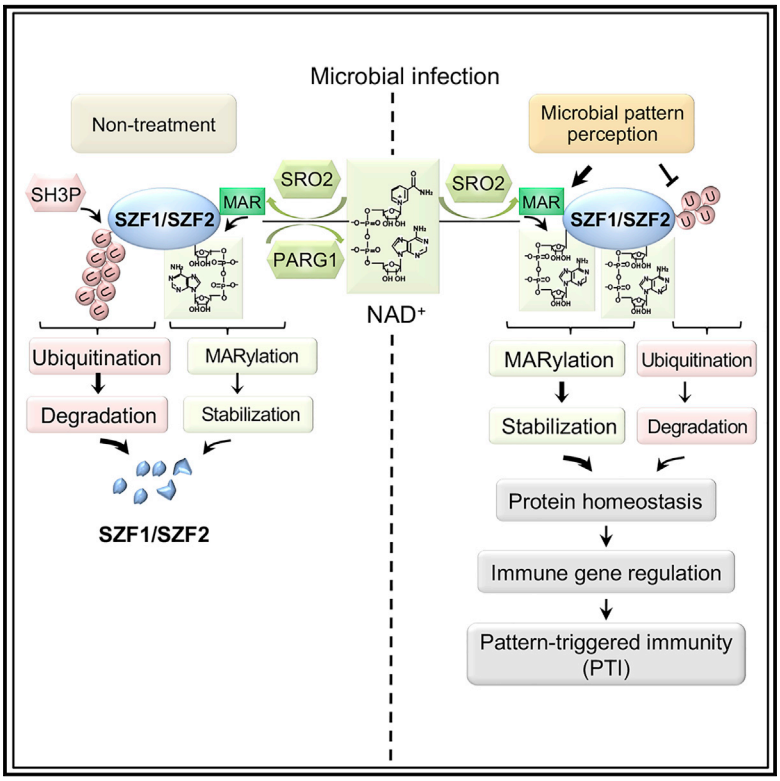

Highlights

- Immune activation promotes ADP-ribosyltransferase SRO2-mediated SZF1/SZF2 MARylation
- MARylation antagonizes SH3P-mediated polyubiquitination to stabilize SZF1
- *Arabidopsis* PARG1 hydrolyzes both PAR and MAR from acceptor proteins
- MARylation of SZF1/SZF2 is essential for plant defense against infection

Authors

Liang Kong, Baomin Feng, Yan Yan, ..., Ivan Ahel, Libo Shan, Ping He

Correspondence

pinghe@tamu.edu

In brief

Kong et al. demonstrate that the noncanonical ADP-ribosyltransferase SRO2 MARylates plant immune regulators SZF1/SZF2 at multiple Asp and Glu residues. Upon immune activation, MARylation of SZF1 antagonizes its polyubiquitination mediated by SH3Ps, thereby stabilizing SZF1 protein and ensuring a proper activation of the immune response.

Kong et al., 2021, Molecular Cell *81*, 1–14
November 18, 2021
https://doi.org/10.1016/j.molcel.2021.09.006

CellPress

Please cite this article in press as: Kong et al., Noncanonical mono(ADP-ribosyl)ation of zinc finger SZF proteins counteracts ubiquitination for protein homeostasis in plant immunity, Molecular Cell (2021), https://doi.org/10.1016/j.molcel.2021.09.006

Molecular Cell

CellPress

Article

Noncanonical mono(ADP-ribosyl)ation of zinc finger SZF proteins counteracts ubiquitination for protein homeostasis in plant immunity

Liang Kong,[1,7] Baomin Feng,[1,2,7] Yan Yan,[1] Chao Zhang,[1,3] Jun Hyeok Kim,[1] Lahong Xu,[1] Johannes Gregor Matthias Rack,[4] Ying Wang,[5] Jyan-Chyun Jang,[6] Ivan Ahel,[4] Libo Shan,[1] and Ping He[1,8,*]

[1]Department of Biochemistry and Biophysics, Texas A&M University, College Station, TX 77843, USA
[2]State Key Laboratory of Ecological Control of Fujian-Taiwan Crop Pests, Key Laboratory of Ministry of Education for Genetics, Breeding and Multiple Utilization of Crops, Plant Immunity Center, Fujian Agriculture and Forestry University, Fuzhou 350002, P.R. China
[3]Department of Plant Pathology and Microbiology, Texas A&M University, College Station, TX 77843, USA
[4]Sir William Dunn School of Pathology, University of Oxford, Oxford OX1 3RE, UK
[5]Department of Biological Sciences, Mississippi State University, Starkville, MS 39762, USA
[6]Department of Horticulture and Crop Science, Department of Molecular Genetics, Center for Applied Plant Sciences, and Center for RNA Biology, The Ohio State University, Columbus, OH 43210, USA
[7]These authors contributed equally
[8]Lead contact
*Correspondence: pinghe@tamu.edu
https://doi.org/10.1016/j.molcel.2021.09.006

SUMMARY

Protein ADP-ribosylation is a reversible post-translational modification that transfers ADP-ribose from NAD^+ onto acceptor proteins. Poly(ADP-ribosyl)ation (PARylation), catalyzed by poly(ADP-ribose) polymerases (PARPs) and poly(ADP-ribose) glycohydrolases (PARGs), which remove the modification, regulates diverse cellular processes. However, the chemistry and physiological functions of mono(ADP-ribosyl)ation (MARylation) remain elusive. Here, we report that *Arabidopsis* zinc finger proteins SZF1 and SZF2, key regulators of immune gene expression, are MARylated by the noncanonical ADP-ribosyltransferase SRO2. Immune elicitation promotes MARylation of SZF1/SZF2 via dissociation from PARG1, which has an unconventional activity in hydrolyzing both poly(ADP-ribose) and mono(ADP-ribose) from acceptor proteins. MARylation antagonizes polyubiquitination of SZF1 mediated by the SH3 domain-containing proteins SH3P1/SH3P2, thereby stabilizing SZF1 proteins. Our study uncovers a noncanonical ADP-ribosyltransferase mediating MARylation of immune regulators and underpins the molecular mechanism of maintaining protein homeostasis by the counter-regulation of ADP-ribosylation and polyubiquitination to ensure proper immune responses.

INTRODUCTION

Plants have evolved complex defense networks in response to microbial attacks (Jones and Dangl, 2006; Zhang et al., 2020; Zhou and Zhang, 2020). The first layer of plant immunity, termed pattern-triggered immunity (PTI), is activated via recognition of pathogen-associated molecular patterns (PAMPs), microbe-associated molecular patterns (MAMPs), or damage-associated molecular patterns (DAMPs) by pattern-recognition receptors (PRRs) (Albert et al., 2020; Couto and Zipfel, 2016; Yu et al., 2017). Plant PRRs are plasma membrane-resident receptor-like kinases (RLKs) and receptor-like proteins (RLPs) (Albert et al., 2020; Couto and Zipfel, 2016; Escocard de Azevedo Manhães et al., 2021; Yu et al., 2017). Activation of PRRs triggers calcium influx, reactive oxygen species (ROS) burst, activation of receptor-like cytoplasmic kinases (RLCKs), calcium-dependent protein kinases (CDPKs), and mitogen-activated protein kinase (MAPK) cascades, transcriptional reprogramming, and callose deposition to strengthen cell wall (Couto and Zipfel, 2016; Yu et al., 2017).

Protein ADP-ribosylation is a reversible post-translational modification that regulates diverse cellular pathways across all domains of life (Bai, 2015; Kraus, 2020; Perina et al., 2014). This process is mediated by ADP-ribosyltransferases (ARTs), which transfer single ADP-ribose (MAR [mono-ADP-ribose]) or multiple ADP-ribose (PAR [poly-ADP-ribose]) from NAD^+ to acceptor proteins, termed mono(ADP-ribosyl)ation (MARylation) or poly(ADP-ribosyl)ation (PARylation), respectively (Cohen and Chang, 2018; Feijs et al., 2013). Humans have 17 diphtheria toxin-type ARTs (ARTDs), also called poly(ADP-ribose) polymerases (PARPs). However, only PARP1 and PARP2 mediate protein PARylation, whereas the rest of human PARPs are either mono- or oligo-ARTs or have no detectable activities (Feijs et al., 2013; Hottiger, 2015). The covalently attached PAR on

Please cite this article in press as: Kong et al., Noncanonical mono(ADP-ribosyl)ation of zinc finger SZF proteins counteracts ubiquitination for protein homeostasis in plant immunity, Molecular Cell (2021), https://doi.org/10.1016/j.molcel.2021.09.006

acceptor proteins could be removed by hydrolases, including poly(ADP-ribose) glycohydrolase (PARG) and (ADP-ribosyl)hydrolases (ARHs); the terminal ADP-ribose, or MAR, can be hydrolyzed by specific macrodomain proteins, such as MacroD1, MacroD2, and the terminal ADP-ribose protein glycohydrolase (TARG1) in mammals (Cohen and Chang, 2018; Rack et al., 2020).

In contrast to the expanded number of PARPs in humans, *Arabidopsis* encodes three *PARPs* (*PARP1–3*) with the conserved ARTD motif (Briggs and Bent, 2011; Feng et al., 2016a; Lamb et al., 2012). Both PARP1 and PARP2 carry PAR polymerase activities and catalyze protein PARylation (Feng et al., 2015; Song et al., 2015). PARP3 is primarily expressed in seeds and is likely enzymatically inactive (Rissel et al., 2014). *Arabidopsis* contains two *PARGs* (*PARG1–2*). PARG1 possesses glycohydrolase activities toward PAR, and PARG2 bears a polymorphism in the PARG signature motif and is thus unlikely to be enzymatically active (Feng et al., 2015; Zhang et al., 2015). In addition, land plants have evolved a group of conserved but plant-specific PARP-like proteins, namely, Radical-induced Cell Death 1 (RCD1) and Similar to RCD 1 (SROs), which are involved in stress adaption and development (Jaspers et al., 2010; Lamb et al., 2012). However, *Arabidopsis* RCD1 lacks PARP activities because of the polymorphism in the conserved ART catalytic triad (Jaspers et al., 2010; Wirthmueller et al., 2018). A recent study suggests that *Arabidopsis* RCD1 likely functions as a PAR reader (Vainonen et al., 2021).

In this study, we identified Salt-inducible Zinc Finger 1 (SZF1) and SZF2, members of Tandem CCCH Zinc Finger (TZF) family proteins, also named TZF11 and TZF10, respectively, as interacting proteins of PARG1. TZFs are conserved from yeast to plants and metazoans with the prototypic human Tristetraprolin (hTTP) involved in gene regulation (Heck and Wilusz, 2018). Perception of MAMPs promotes the release of SZF1/SZF2 from PARG1, resulting in the increased ADP-ribosylation of SZF1/SZF2. ADP-ribosylation of SZF1/SZF2 could be removed by PARG1 but occurs independently of PARPs. The noncanonical ART SRO2 directly MARylates SZF1/SZF2, and SRO2-mediated MARylation increases the protein stability of SZF1, which is otherwise polyubiquitinated and destabilized by the SH3 domain-containing proteins SH3P1 and SH3P2. We report a plant ART functioning in protein MARylation, which counteracts polyubiquitination to regulate protein homeostasis, and a notable role of PARG in hydrolyzing MAR.

RESULTS

SZF1 and SZF2 interact with PARG1

To understand the role of PARylation in plant immunity, we performed a yeast two-hybrid screen using an *Arabidopsis* cDNA library to identify PARG1-interacting proteins. SZF1 was identified from our screen (Figure 1A). SZF1, together with its homolog SZF2, contains two zinc finger (ZnF) motifs and two ankyrin repeat (ANK) domains (Figures S1A–S1C) (Jang, 2016). Co-immunoprecipitation (co-IP) assays showed that SZF1 and SZF2 immunoprecipitated PARG1 in *Arabidopsis* protoplasts (Figures 1B and S1D). The association between PARG1 and SZF1/SZF2 was reduced upon flg22 treatment (Figure 1B), a 22 amino acid peptide from bacterial flagellin. The association and flg22-induced dissociation of PARG1 and SZF1 were confirmed in transgenic plants expressing *SZF1-FLAG* under its native promoter and *PARG1-HA* under the *35S* promoter (Figure S1E). An *in vitro* pull-down assay indicates that GST-tagged PARG1, but not GST-tagged MBP, directly pulled down HIS-tagged SZF1/SZF2 (Figure 1C). Moreover, Förster resonance energy transfer (FRET)-fluorescence lifetime imaging (FLIM) experiments revealed that SZF1/SZF2-GFP were in the close vicinity of PARG1-mCherry, but not DAWDLE (DDL)-mCherry, a plant ADP-ribosylated protein (Feng et al., 2016b) (Figures 1D and 1E). CoIP assays with different SZF1 truncations showed that PARG1 co-immunoprecipitated with SZF1 C terminus ($SZF1^{C}$) but not N terminus ($SZF1^{N}$) or C terminus without ZnF ($SZF1^{C\Delta ZnF}$) (Figures S1F and S1G), indicating that both ZnF and C-terminal domains are essential for SZF1 interaction with PARG1.

PARG1 localized in the nucleus and cytoplasm in *Arabidopsis* protoplasts (Figure 1F). SZF1-GFP also accumulated in the nucleus and cytoplasm with high co-localization efficiency with PARG1-mCherry (Figures 1F and 1G). Fluorescence intensity profiles of the cross-section confirmed the nuclear signal of PARG1-GFP and SZF1-GFP overlapping with that of nuclear-localized RFP (NLS-RFP) (Figure 1G). Additionally, SZF1-GFP accumulated in cytoplasmic puncta, which partially co-localized with DECAPPING 1 (DCP1)-mCherry, a processing body (P-body) marker (Yu et al., 2019a) (Figures 1F, 1G, and S1H). The nucleus and cytoplasmic puncta localization of SZF1/SZF2-GFP was also observed in *Arabidopsis* transgenic plants (Figure 1H). Thus, SZF1/SZF2 may function together with PARG1 in the nucleus and cytoplasm.

Immune elicitation promotes ADP-ribosylation of SZF1/SZF2

Given that SZF1/SZF2 interacted with PARG1, we tested whether SZF1/SZF2 were ADP-ribosylated. When incubating GST-SZF1 or GST-SZF2 with plant extracts and biotin-NAD^+, ADP-ribosylated SZF1/SZF2 proteins were detected by immunoblotting using horseradish peroxidase (HRP)-conjugated streptavidin for biotinylated NAD^+ (Figure 2A). When expressing SZF1/SZF2-HA in protoplasts, macrodomain affinity (MD) resins, which bind MARylated or PARylated proteins (Daniels et al., 2014), could enrich both SZF1-HA and SZF2-HA (Figure 2B). Treatment of flg22, not salt, enhanced SZF ADP-ribosylation (Figure 2B). The flg22-induced SZF1 ADP-ribosylation was observed as early as 0.5 h after treatment (Figure S2A). In addition, when protoplasts expressing SZF1-FLAG were fed with radiolabeled ^{32}P-NAD^+, ADP-ribosylated SZF1-FLAG was evident with the autoradiograph after α-FLAG immunoprecipitation and was enhanced upon flg22 treatment (Figure 2C). The molecular weight increase of ADP-ribosylated SZF1 was not as pronounced as that of DDL, which is PARylated (Figure 2C) (Feng et al., 2016b). Together, the data indicate that flg22 treatment stimulates ADP-ribosylation of SZF1/SZF2.

PARPs do not ADP-ribosylate SZF1, but PARG1 removes SZF1 ADP-ribosylation

Next, we investigated whether SZF1 ADP-ribosylation is mediated by PARPs and can be removed by PARG1. We compared SZF1

Please cite this article in press as: Kong et al., Noncanonical mono(ADP-ribosyl)ation of zinc finger SZF proteins counteracts ubiquitination for protein homeostasis in plant immunity, Molecular Cell (2021), https://doi.org/10.1016/j.molcel.2021.09.006

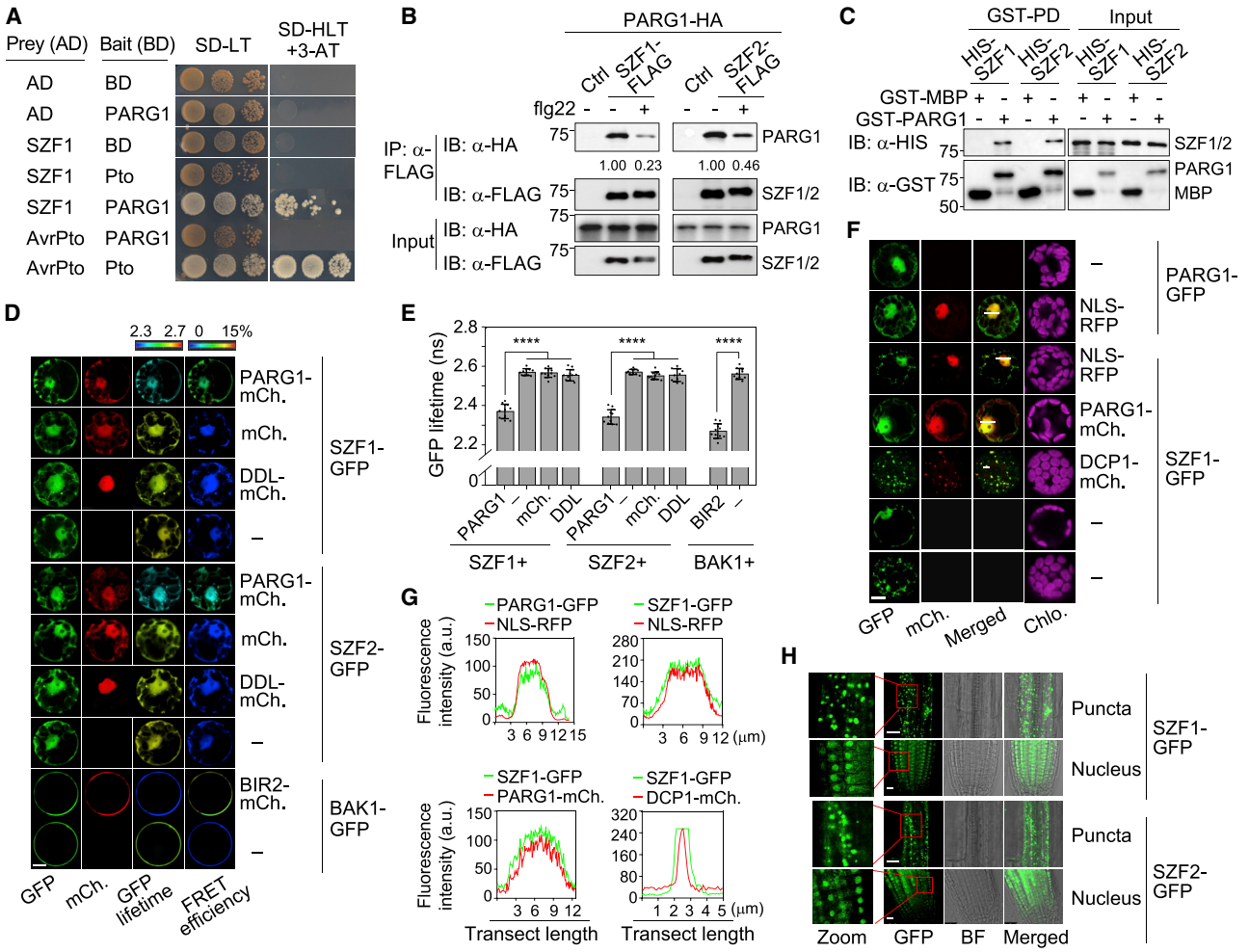

Figure 1. PARG1 interacts with SZF1/SZF2 and colocalizes with SZF1

(A) PARG1 interacts with SZF1 in yeast. Yeast was grown on synthetic drop-out medium without Leu and Trp (SD-LT) and His, Leu, and Trp (SD-HLT) supplemented with 1 mM 3-AT. pGADT7 (AD) and pGBKT7 (BD) are empty vectors, and AvrPto and Pto are controls.

(B) PARG1 associates with SZF1/SZF2 in *Arabidopsis* protoplasts. Protoplasts from WT plants were transfected with PARG1-HA and SZF1/2-FLAG, or control vector (Ctrl), and treated with or without 0.1 μM flg22 for 1 h. Co-immunoprecipitation (coIP) assays were carried out with α-FLAG agarose and followed by immunoblotting (IB) with α-HA or α-FLAG antibody (top two) with input proteins shown (bottom two). The molecular weight (kDa) was labeled on the left of the images (same for other immunoblots). Relative band intensities of immunoprecipitated proteins normalized to input proteins were labeled. The value of samples without flg22 treatment was set as 1.0.

(C) PARG1 interacts with SZF1/SZF2 in pull-down assays. GST-MBP or GST-PARG1 proteins immobilized on glutathione Sepharose were incubated with HIS-SZF1/SZF2 followed by washing and IB with α-HIS or α-GST antibody.

(D and E) PARG1 interacts with SZF1/SZF2 in FRET-FLIM assays. (D) Localization of SZF1/SZF2-GFP and PARG1-mCherry in protoplasts is shown in the first and second columns, respectively. Lifetime (τ) distribution (third) and apparent FRET efficiency (fourth) are presented as pseudocolor images according to the scale. Scale bar, 10 μm. (E) GFP mean fluorescence lifetime (τ) values (nanoseconds) were statistically analyzed and are shown as an overlay of dot plot with mean ± SD; n = 10. Asterisks represent significant differences (****$p < 0.0001$, one-way ANOVA). DDL, BAK1, and BIR2 are controls.

(F and G) SZF1-GFP localizes in the nucleus and P-bodies in protoplasts. DCP1-mCherry and NLS-RFP are P-body and nuclear markers, respectively. (F) Cells were imaged using a GFP, mCherry, or chlorophyll autofluorescence filter under a laser-scanning confocal microscope (LSCM). Scale bar, 10 μm. (G) Fluorescence intensity profiles of GFP and mCherry are assessed in the nucleus and puncta transect shown in the third column of (F) (white line).

(H) SZF1/SZF2-GFP localize in the nucleus and cytoplasmic puncta in transgenic plants. Roots from 10-day-old *p35S::SZF1/SZF2-GFP* transgenic plants were imaged under an LSCM with zoom inserts on the left. Scale bar, 10 μm.

Experiments were repeated three times with similar results. See also Figure S1.

ADP-ribosylation in wild-type (WT), *parg1*, or *parp1,2* mutants. The level of SZF1 ADP-ribosylation, detected by radiolabeled ^{32}P-NAD$^+$ as the ADP-ribose donor, increased in *parg1* but did not change in *parp1,2* compared with WT (Figure 2D). Consistent with the previous report (Feng et al., 2016b), PARylation of DDL increased in *parg1* but reduced in *parp1,2* (Figure 2D). The level of ADP-ribosylated GST-SZF1 detected by streptavidin-HRP (Figure 2E) or ^{32}P-NAD$^+$ autoradiograph (Figure 2F) increased when

Please cite this article in press as: Kong et al., Noncanonical mono(ADP-ribosyl)ation of zinc finger SZF proteins counteracts ubiquitination for protein homeostasis in plant immunity, Molecular Cell (2021), https://doi.org/10.1016/j.molcel.2021.09.006

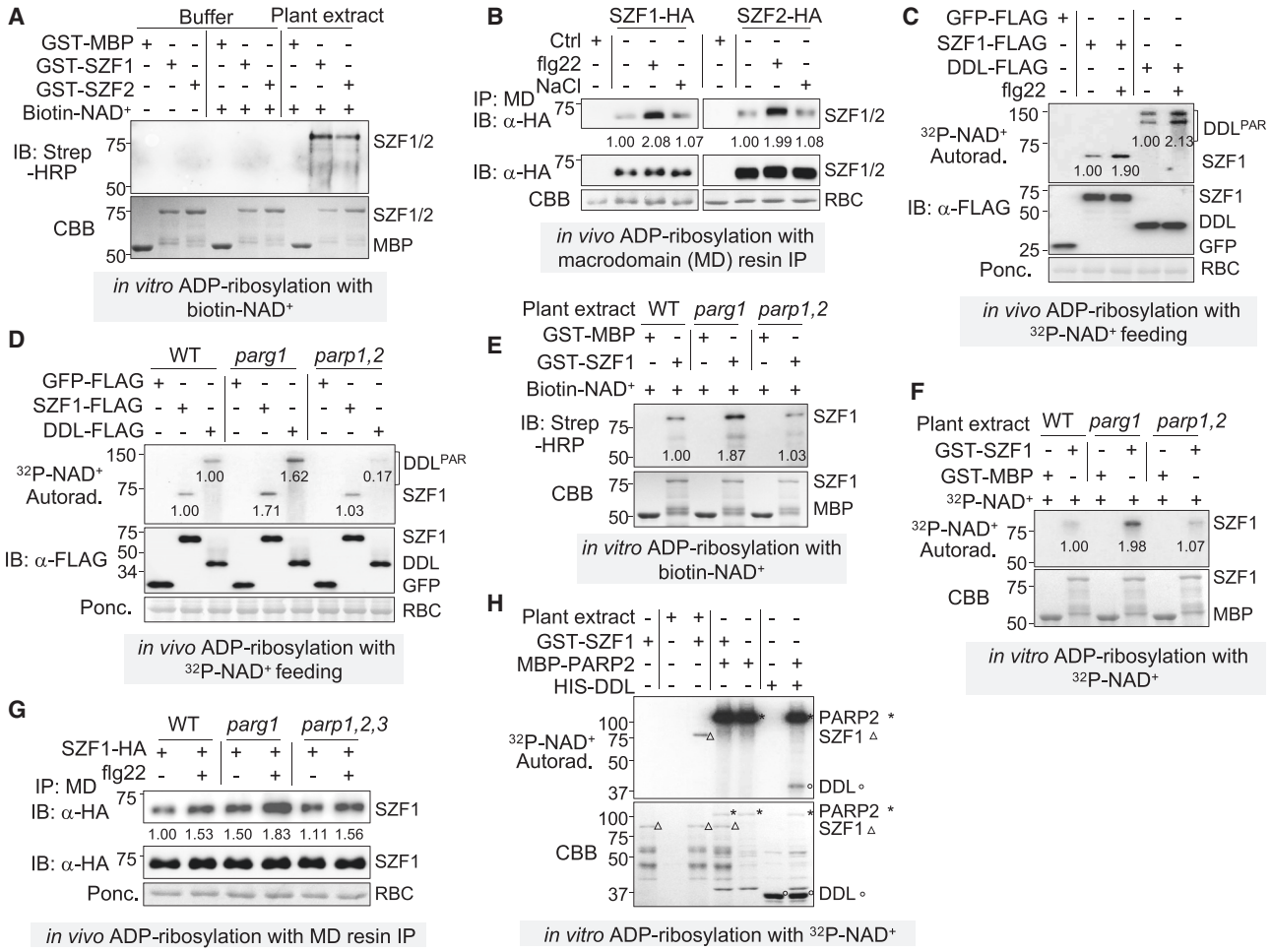

Figure 2. Flg22 induces ADP-ribosylation of SZF1/SZF2 in a PARG1-dependent manner

(A) SZF1/SZF2 are ADP-ribosylated in the presence of plant extracts. GST-SZF1/SZF2 and GST-MBP proteins immobilized on glutathione Sepharose were incubated with or without plant extracts in an ADP-ribosylation reaction containing biotin-NAD$^+$. ADP-ribosylated proteins were detected by streptavidin-HRP (Strep-HRP). Coomassie Brilliant Blue (CBB) staining shows protein loading.

(B) Treatment of flg22, not salt, induces ADP-ribosylation of SZF1/SZF2. Protoplasts expressing SZF1/SZF2-HA were treated with 0.1 μM flg22 or 1 mM NaCl for 1 h. Ribosylated proteins were immunoprecipitated using MD resins followed by IB using α-HA antibody (top). Input proteins are shown in the middle panel. CBB shows protein loading for Rubisco (RBC).

(C) Flg22 treatment induces SZF1 ADP-ribosylation. Protoplasts expressing SZF1-FLAG, DDL-FLAG, or GFP-FLAG were fed with ^{32}P-NAD$^+$ for 1 h, followed by 1 h treatment with 0.1 μM flg22. After IP using α-FLAG antibody, ADP-ribosylated proteins were detected by autoradiography (top). Input proteins are shown by α-FLAG IB (middle). Ponceau S staining of RBC for protein loading (bottom).

(D) SZF1 ADP-ribosylation is enhanced in *parg1* but not in *parp1,2*. Experiments were performed as in (C) using protoplasts from WT, *parg1*, or *parp1,2*.

(E and F) SZF1 ADP-ribosylation is enhanced with *parg1* plant extracts. GST-SZF1 or GST-MBP proteins immobilized on glutathione Sepharose were incubated with plant extracts in an ADP-ribosylation reaction containing biotinylated NAD$^+$ (E) or ^{32}P-NAD$^+$ (F). ADP-ribosylated SZF1 was detected by Strep-HRP (E) or autoradiography (F).

(G) Flg22-induced SZF1 ADP-ribosylation is enhanced in *parg1*. Experiments were performed as in (B) using protoplasts from WT, *parg1*, or *parp1,2,3*.

(H) PARP2 ADP-ribosylates DDL but not SZF1. GST-SZF1 or HIS-DDL proteins were incubated with MBP-PARP2 or plant extracts in an ADP-ribosylation reaction containing ^{32}P-NAD$^+$.

Relative band intensities of ADP-ribosylated proteins normalized to input proteins are labeled in (B)–(G). The value of samples without treatment or in WT was set as 1.0. Experiments were repeated three times in (A)–(C), (E), (F), and (H) and twice in (D) and (G) with similar results. See also Figure S2.

incubating with plant extracts of *parg1*, but it did not change with plant extracts from *parp1,2*. To exclude the potential function of PARP3, we generated the *parp1,2,3* triple mutant (Figure S2B). Similarly, the amount of MD resin-immunoprecipitated SZF1 proteins increased in *parg1* but did not change in *parp1,2,3* (Figure 2G). Co-incubation of *parp1,2,3* plant extracts also did not affect ADP-ribosylation of GST-SZF1 (Figure S2C). The data collectively indicate that PARPs do not mediate ADP-ribosylation of SZF1, but PARG1 removes ADP-ribose attached to SZF1. In contrast, PARP2 directly ADP-ribosylated DDL, but not SZF1 (Figure 2H). Furthermore, unlike PARG1, PARP2 did not directly interact with SZF1/SZF2 in an *in vitro* pull-down assay (Figure S2D).

Please cite this article in press as: Kong et al., Noncanonical mono(ADP-ribosyl)ation of zinc finger SZF proteins counteracts ubiquitination for protein homeostasis in plant immunity, Molecular Cell (2021), https://doi.org/10.1016/j.molcel.2021.09.006

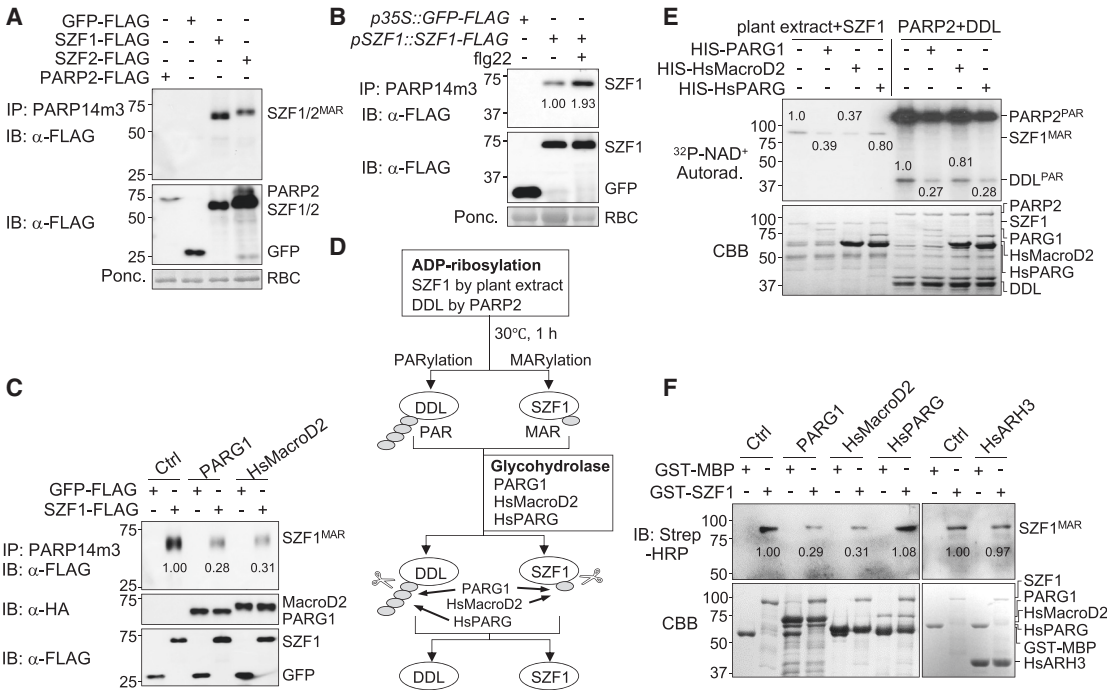

Figure 3. SZF1 undergoes PARG1-dependent MARylation in plants

(A) SZF1/SZF2 are MARylated in plants. Protoplasts expressing SZF1-FLAG, SZF2-FLAG, PAPR2-FLAG, or GFP-FLAG were immunoprecipitated with PARP14m3 resins followed by IB using α-FLAG antibody (top) with input proteins shown by α-FLAG IB before IP (middle) and protein loading by Ponceau S staining (bottom).

(B) Flg22 induces SZF1 MARylation in transgenic plants. Protein extracts from transgenic plants carrying *SZF1* or *GFP* were subjected for IP with PARP14m3 resins and IB with α-FLAG antibody (top). Input proteins are shown by α-FLAG IB (middle) and Ponceau S staining for protein loading (bottom). Relative band intensities of ADP-ribosylated proteins normalized to input proteins were labeled (no flg22 treatment was set as 1.0).

(C) PARG1 and HsMacroD2 reduce SZF1 MARylation. Protoplasts were expressed with SZF1-FLAG or GFP-FLAG with PARG1-HA, HsMacroD2-HA, or an empty vector (Ctrl). IP and IB were performed as in (A). Relative band intensities of ADP-ribosylated proteins normalized to input proteins were labeled (SZF1 without hydrolases was set as 1.0).

(D) Diagram of removal of MAR or PAR by PARG1, HsPARG, or HsMacroD2 from MARylated SZF1 or PARylated DDL.

(E) SZF1 MARylation could be removed by PARG1 and HsMacroD2, but not by HsPARG. GST-SZF1 was MARylated by co-incubating plant extracts containing ^{32}P-NAD$^+$. HIS-DDL was PARylated by MBP-PARP2. MARylated SZF1 or PARylated DDL was then incubated with HIS-PARG1, HIS-HsMacroD2, or HIS-HsPARG. Quantification of SZF1 or DDL ADP-ribosylation was labeled.

(F) PARG1 and HsMacroD2, not HsPARG nor HsARH3, remove MAR from SZF1. GST-SZF1 or GST-MBP was incubated with plant extracts containing biotin-NAD$^+$. MARylated SZF1 was incubated with HIS-PARG1, HIS-HsMacroD2, HIS-HsPARG, or HIS-HsARH3. Quantification of SZF1 ADP-ribosylation was labeled. Experiments were repeated at least three times with similar results. See also Figure S2.

SZF1/SZF2 are MARylated, which can be removed by PARG1

These observations prompted us to hypothesize that SZF1 ADP-ribosylation might be MARylation but not PARylation. Consistently, the α-PAR antibody, which recognizes PAR polymers of PARylated proteins, detected PARylated PARP2, but not SZF1/SZF2 (Figure S2E). Additionally, SZF1/SZF2, but not PARP2, could be immunoprecipitated by PARP14m3 resins, which only bind MARylated proteins (Vyas et al., 2014) (Figure 3A), suggesting that SZF1/SZF2 were MARylated in plants. Similarly, SZF1 was immunoprecipitated by PARP14m3 resins from transgenic plants expressing *SZF1* under its native promoter, and SZF1 MARylation was enhanced upon flg22 treatment (Figure 3B). HopF2, a mono-ART from bacterium *Pseudomonas syringae* (Wang et al., 2010), served as a positive control, was also immunoprecipitated by PARP14m3 resins (Figure S2F).

Expressing PARG1-HA reduced SZF1 MARylation detected by PARP14m3 resins (Figure 3C), indicating that PARG1 could remove MAR from MARylated SZF1. Furthermore, human MacroD2-HA, a MAR hydrolase (Rack et al., 2020; Rosenthal et al., 2013), reduced SZF1 MARylation (Figure 3C), supporting that SZF1 ADP-ribosylation is MARylation. Additionally, HIS-PARG1 reduced MARylation level of GST-SZF1 detected by ^{32}P-NAD$^+$ autoradiography (Figures 3D and 3E) or streptavidin-HRP (Figure 3F). Similarly, MARylated SZF1 was partially removed by HIS-MacroD2, but not much by human PARG, a PAR glycohydrolase (Figures 3E and 3F). In contrast, PARG1 and human PARG, but not MacroD2, hydrolyzed PARP2-PARylated DDL (Figures 3D and 3E). Interestingly, human ARH3, which prefers Ser-linked ADP-ribosylation (Fontana et al., 2017), had little effect on SZF1 MARylation (Figure 3F). As MacroD2 mainly removes Asp- and Glu-linked MAR (Rosenthal et al., 2013), likely, SZF1 MARylation is mostly Asp and Glu linked. Together, the

Please cite this article in press as: Kong et al., Noncanonical mono(ADP-ribosyl)ation of zinc finger SZF proteins counteracts ubiquitination for protein homeostasis in plant immunity, Molecular Cell (2021), https://doi.org/10.1016/j.molcel.2021.09.006

data support that SZF1 is MARylated in plants, and *Arabidopsis* PARG1 is a glycohydrolase that removes both PAR and MAR from acceptor proteins (Figure 3D).

SRO2 MARylates SZF1/SZF2 at multiple Asp and Glu residues

To identify the mono-ART(s) that MARylates SZF1/SZF2, we focused on plant-specific PARP-like proteins RCD1/SROs. *Arabidopsis* encodes one *RCD1* and five *SRO*s clustered into three groups that are phylogenetically closer to human mono-ARTs PARP14/16 than poly-ARTs (Figure S3A). We cloned RCD1, SRO2, and SRO5, representing each group to examine their ART activities. SRO2, but not RCD1 or SRO5, was immunoprecipitated by MD resins (Figure 4A). Furthermore, SRO2, but not PARP2, was immunoprecipitated by PARP14m3 resins (Figure 4A), indicative of SRO2 MARylation *in planta*. An *in vitro* ADP-ribosylation assay showed that HIS-SRO2, but not HIS-DDL, was auto-ADP-ribosylated (Figure 4B), indicating that SRO2 has mono-ART activities. Additionally, ADP-ribosylated SRO2 could be hydrolyzed by *Arabidopsis* PARG1 and human MacroD2 (Figure 4B), further supporting that *Arabidopsis* PARG1 bears MAR hydrolysis activities.

HIS-SRO2 was immunoprecipitated by GST-SZF1/SZF2, but not GST, in an *in vitro* pull-down assay (Figure 4C). The interaction between SRO2 and SZF1/SZF2 was confirmed by *in vivo* co-IP assays in protoplasts (Figure S3B) and transgenic plants carrying *SRO2* and *SZF1/SZF2* (Figure 4D). Flg22 treatment did not affect SRO2-SZF1/SZF2 interactions (Figures 4D and S3B). Moreover, HIS-SRO2 MARylated GST-SZF1/SZF2 *in vitro* and PARG1 removed SRO2-mediated SZF1/SZF2 MARylation (Figures 4E and S3C). Furthermore, MARylated SZF1/SZF2 were substantially reduced in *sro2-2*, and flg22-induced SZF1 MARylation did not occur in *sro2-2* (Figures 4F and S3D). Consistently, MARylation of GST-SZF1/SZF2 was considerably reduced in *sro2-2* compared with WT plants (Figure S3E). The data demonstrated that SRO2 directly binds and MARylates SZF1/SZF2.

To identify MARylated residues, we deployed liquid chromatography-tandem mass spectrometry (LC-MS/MS) analysis (Feng et al., 2016b) with SZF1/SZF2 proteins incubated with SRO2 and plant extracts. For SZF1, among 1,104 peptides detected (~75% coverage), 8 peptides with nine MARylated Glu or Asp residues were identified (Figures 4G–4I and S3F–S3I; Table S1). Four residues are in the N terminus, three between ANK and ZnF domains, and two in the first ZnF domain of SZF1 (Figure 4H). For SZF2, among 2,061 peptides detected (~87% coverage), 12 MARylated Glu and Asp sites from 7 peptides were identified (Figures 4H and S4A–S4H; Table S1). Four residues are in the N terminus and ANK domain, five between ANK and ZnF domains, two in the first ZnF domain, and one in the C terminus (Figure 4H). Many MARylated sites of SZF1 (E25, D37, D229, E232, D269, E272) and SZF2 (E25, D41, D232, E235, D272, E275) are conserved (Figure 4H). To examine whether these sites are required for SZF1 MARylation, we mutated all nine Asp (D) and Glu (E) residues to Ala (A) (hereafter designated SZF1^{mDE}). Notably, SZF1^{mDE} MARylation was lower than SZF1, and flg22 treatment did not induce SZF1^{mDE} MARylation in *Arabidopsis* protoplasts (Figure S4I). Additionally, MARylation of SZF1^{mDE} was reduced in *pSZF1::SZF1^{mDE}-FLAG* transgenic plants (Figure 4J). Thus, Glu and Asp residues identified by LC-MS/MS are required for SZF1 MARylation.

Immune elicitation stabilizes SZF1 proteins

We observed that SZF1 protein levels were increased markedly after flg22 treatment in *pSZF1::SZF1-FLAG* or *pSZF1::SZF1-GFP* transgenic plants (Figures 5A and S5A). Similarly, treatment of nonpathogenic *P. syringae* pv. *tomato* (*Pst*) DC3000 *hrcC* induced SZF1 protein accumulation (Figure 5B). However, *SZF1/SZF2* transcripts did not change significantly after flg22 treatment (Figure S5B). Although *SZF1/SZF2* were transcriptionally upregulated by salt (Sun et al., 2007), SZF1 proteins were substantially reduced after salt treatment (Figure 5C). This contrasts with increased SZF1 proteins upon flg22 treatment. Furthermore, when treating *p35S::SZF1-FLAG* transgenic plants with flg22, SZF1 proteins were also increased (Figure 5D), supporting a posttranscriptional regulation of flg22-induced SZF1 protein accumulation. Notably, MG132, a proteasome inhibitor, stabilized SZF1 to a similar level as the flg22 treatment (Figure 5E). Together, the data suggest that SZF1 is degraded in a proteasome-dependent manner, whereas flg22 treatment stabilizes SZF1 proteins.

To identify proteins regulating SZF1 stability, we performed immunoaffinity purification and LC-MS/MS analysis of SZF1 complexes using *pSZF1::SZF1-FLAG/szf1* seedlings. We mainly focused on candidates with potential functions in protein degradation, including SH3P1 and its homolog SH3P2, E3 ubiquitin ligases (PUB2, MAC3A, and MAC3B) (Figure S5C). We silenced individual candidates in *pSZF1::SZF1-FLAG/szf1* transgenic *Arabidopsis* plants by virus-induced gene silencing (VIGS) (Figures S5D and S5E). Strikingly, SZF1 proteins were higher in *SH3P1*- or *SH3P2*-silenced plants than plants silencing *MAC3A*, *MAC3B*, *PUB2*, or a control vector (Figure 5F). Flg22 treatment did not increase SZF1 proteins in *SH3P1*- or *SH3P2*-silenced plants (Figure 5F). Furthermore, SZF1 proteins were higher in multiple independent *pSZF1::SZF1-HA* transgenic plants in the *sh3p1* mutant than those in WT (Figure 5G). Moreover, SH3P1-FLAG associated with SZF1-HA and flg22 treatment reduced the association in co-IP assays using transgenic plants expressing *SZF1-FLAG* and *SH3P1-HA* (Figure 5H). The SH3 domain binds ubiquitin to mediate protein ubiquitination in mammals (Stamenova et al., 2007). *Arabidopsis* SH3P2 acts as a ubiquitin-binding protein (Nagel et al., 2017), and SH3P1 regulates clathrin-coated vesicular trafficking (Lam et al., 2001). Together, SH3P1/SH3P2-mediated ubiquitination likely regulates SZF1 stability.

MARylation counter-regulates SZF1 ubiquitination and stability

To test whether SZF1 is ubiquitinated *in planta*, we co-expressed SZF1-HA and FLAG-tagged ubiquitin (FLAG-UBQ) in *Arabidopsis* protoplasts. SZF1 polyubiquitination was detected as a ladder-like smear in an α-HA immunoblot after α-FLAG immunoprecipitation (Figure 6A). Flg22 treatment reduced SZF1 ubiquitination (Figure 6A). SZF1 ubiquitination was also detected in *pSZF1::SZF1-GFP* transgenic plants using α-ubiquitin (α-Ubq) antibody after α-GFP immunoprecipitation and was reduced after flg22 treatment (Figure 6B). Moreover, SZF1 ubiquitination

Please cite this article in press as: Kong et al., Noncanonical mono(ADP-ribosyl)ation of zinc finger SZF proteins counteracts ubiquitination for protein homeostasis in plant immunity, Molecular Cell (2021), https://doi.org/10.1016/j.molcel.2021.09.006

CellPress

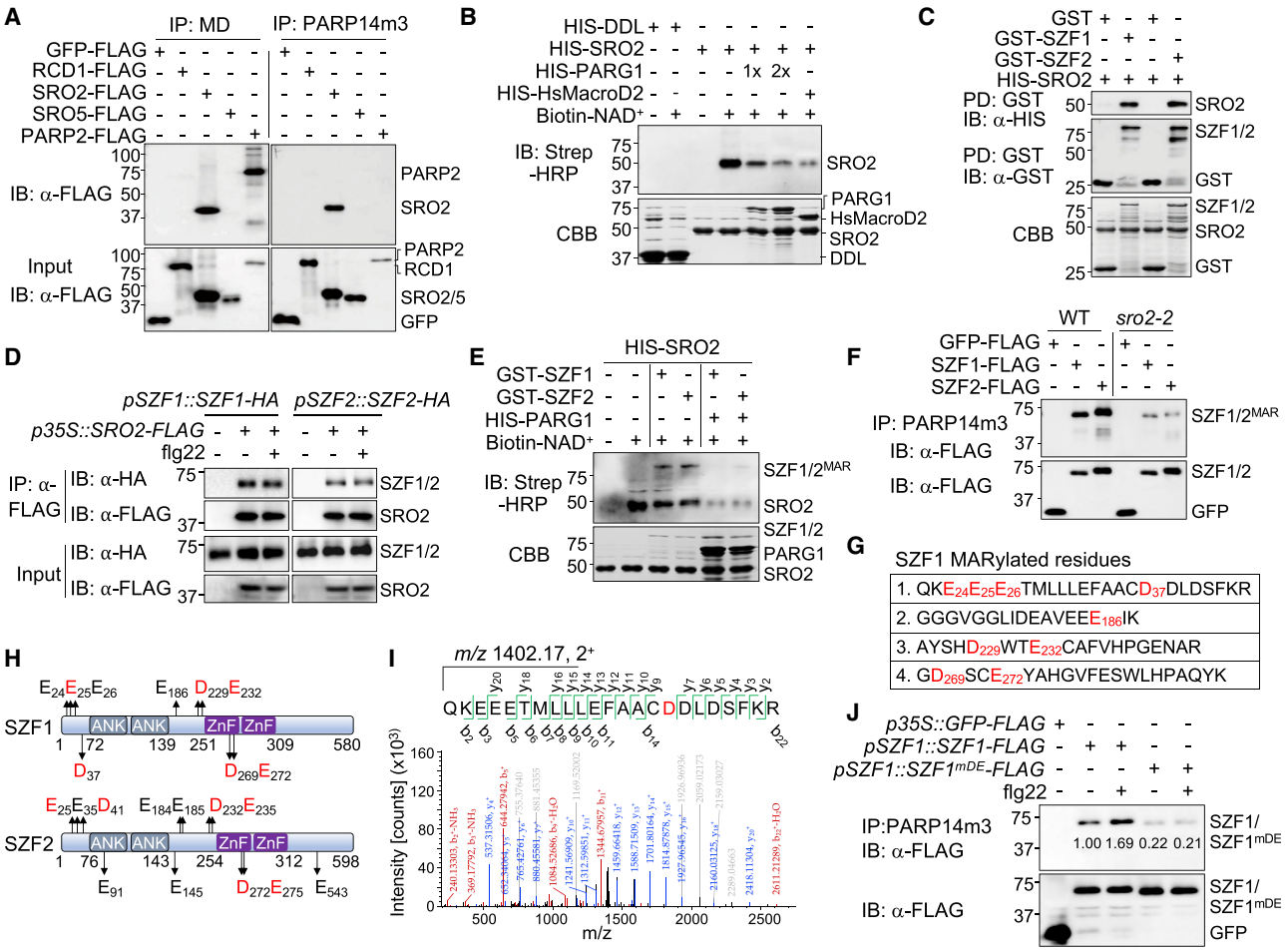

Figure 4. SRO2 MARylates SZF1/SZF2 at Glu and Asp residues

(A) SRO2 is MARylated in plants. Proteins expressed in protoplasts were immunoprecipitated using MD resins or PARP14m3 resins and followed by α-FLAG IB (top). Input proteins are shown by α-FLAG IB before IP (bottom).

(B) SRO2 auto-MARylation is removed by PARG1 and HsMacroD2. HIS-SRO2 or HIS-DDL was subjected to biotin-NAD^+-mediated APD-ribosylation with or without HIS-PARG1 or HIS-HsMacroD2.

(C) SRO2 interacts with SZF1/SZF2. GST-SZF1/SZF2 or GST immobilized on glutathione Sepharose was incubated with HIS-SRO2, followed by washing and IB with α-HIS (top) or α-GST antibody (middle) with input proteins shown by CBB staining (bottom).

(D) SRO2 associates with SZF1/SZF2 in transgenic plants. Four-week-old transgenic plants expressing *pSZF1::SZF1-HA* or *pSZF2::SZF2-HA* and *p35S::SRO2-FLAG* were treated with 0.1 μM flg22 for 1 h, and protein extracts were subjected for co-IP assay (top two) with input proteins shown (bottom two).

(E) SRO2 MARylates SZF1/SZF2, and PARG1 removes MARylation. GST-SZF1/SZF2 was incubated with HIS-SRO2 in an ADP-ribosylation reaction with biotinylated NAD^+ and followed by incubating with or without HIS-PARG1.

(F) MARylation of SZF1/SZF2 is reduced in *sro2-2*. Protoplasts from WT or *sro2-2* were expressed with SZF1/SZF2-FLAG or GFP-FLAG. IP and IB were performed as in (A).

(G) SRO2 MARylates SZF1 at multiple Glu and Asp residues. MARylated residues in SZF1 identified by LC-MS/MS analysis are shown in red with amino acid positions labeled. See Table S1.

(H) Diagram of SZF1/SZF2 protein motifs with identified MARylated sites. The conserved MARylated residues are marked in red. See Table S1.

(I) MS/MS spectrum of a peptide containing MARylated D37 in SZF1.

(J) MARylation of $SZF1^{mDE}$ is reduced in transgenic plants. Ten-day-old transgenic plants expressing *SZF1* or $SZF1^{mDE}$ under the native promoter were treated with or without 0.1 μM flg22 for 1 h. SZF1 and $SZF1^{mDE}$ input proteins were adjusted to a similar level before IP using PARP14m3 resins. Quantification of ADP-ribosylated SZF1 relative to input proteins was labeled.

Experiments were repeated at least three times with similar results. See also Figures S3 and S4 and Table S1.

was reduced in *pSZF1::SZF1-HA* transgenic plants in *sh3p1* compared with that in WT (Figure S5F), corroborating SH3P1-mediated destabilization of SZF1 by ubiquitination. Thus, flg22 treatment suppresses SH3P-mediated SZF1 polyubiquitination, thereby stabilizing SZF1.

We next investigated the relationship between flg22-induced MARylation and flg22-suppressed polyubiquitination of SZF1. Expression of PARG1, but not PARP2, markedly alleviated flg22-suppressed SZF1 ubiquitination (Figure S5G). In addition, PARG1 substantially increased SZF1 ubiquitination before

Please cite this article in press as: Kong et al., Noncanonical mono(ADP-ribosyl)ation of zinc finger SZF proteins counteracts ubiquitination for protein homeostasis in plant immunity, Molecular Cell (2021), https://doi.org/10.1016/j.molcel.2021.09.006

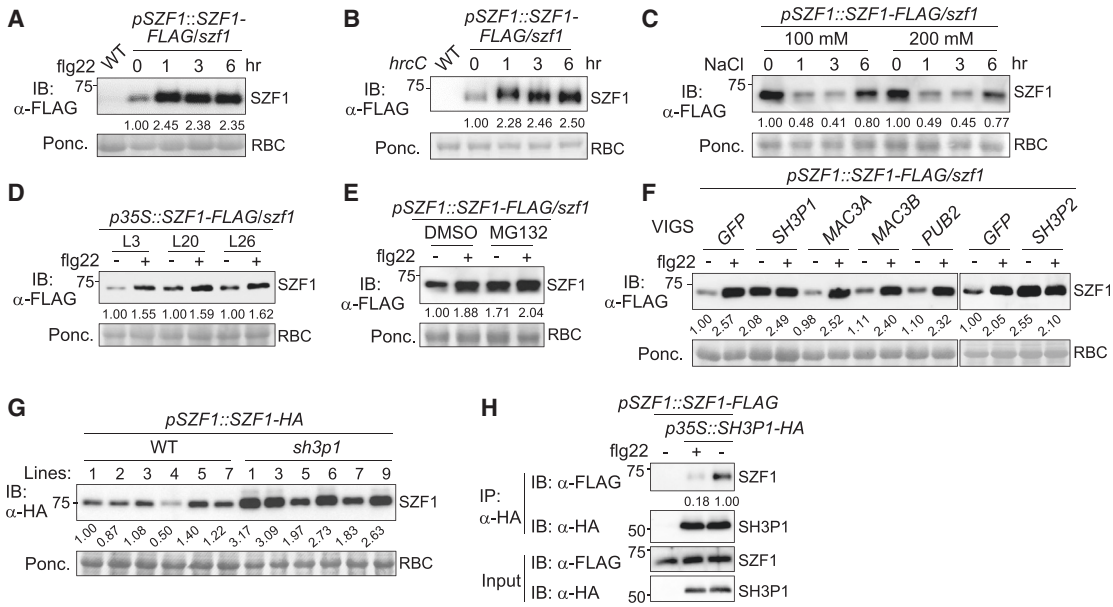

Figure 5. Flg22 treatment modulates SH3P1-dependent SZF1 stability

(A) Flg22 treatment increases SZF1 protein accumulation. Ten-day-old *pSZF1::SZF1-FLAG/szf1* transgenic plants were treated with 0.1 μM flg22 for the indicated time. Protein extracts were subjected to IB using α-FLAG antibody (top) with protein loading shown by Ponceau S staining for RBC (bottom).

(B) Inoculation of *Pst* DC3000 *hrcC* induces SZF1 protein accumulation. Leaves of 4-week-old *pSZF1::SZF1-FLAG/szf1* plants were inoculated with *Pst* DC3000 *hrcC* at OD_{600} = 0.4, and collected at the indicated time for IB.

(C) Salt treatment reduces SZF1 protein accumulation. Ten-day-old seedlings were treated with 100 or 200 mM NaCl.

(D) Flg22 treatment increases SZF1 protein accumulation in *p35S::SZF1-FLAG/szf1* transgenic plants. Ten-day-old seedlings were treated with 0.1 μM flg22 for 1 h. L3, L20, and L26 are independent lines.

(E) Proteasome inhibitor MG132 stabilizes SZF1. Ten-day-old seedlings were pre-treated with MG132 or DMSO for 1 h before 0.1 μM flg22 treatment for 1 h.

(F) Silencing *SH3P1* or *SH3P2* increases SZF1 protein accumulation. *Arabidopsis pSZF1::SZF1-FLAG/szf1* transgenic plants were inoculated with VIGS constructs for silencing *SH3P1*, *SH3P2*, *MAC3A*, *MAC3B*, *PUB2*, or *GFP*. Leaves were collected 2 weeks after VIGS for IB.

(G) SH3P1 regulates SZF1 protein stability. *pSZF1::SZF1-HA* was transformed into WT or *sh3p1*, and multiple independent transgenic plants were obtained for IB using α-HA antibody.

(H) SZF1 associates with SH3P1. Four-week-old transgenic plants expressing *pSZF1::SZF1-FLAG* with and without *p35S::SH3P1-HA* were treated with 0.1 μM flg22 for 1 h, and protein extracts were isolated for coIP assays (top two) with input proteins shown (bottom two). SZF1 input proteins were adjusted to a similar level with and without *p35S::SH3P1-HA* before IP.

Relative band intensities of SZF1 normalized to input proteins were labeled. The value of samples without treatment was set as 1.0 (A–H). Experiments were repeated three times with similar results. See also Figure S5.

flg22 treatment (Figure S5G). Conversely, SZF1 ubiquitination was reduced in *parg1*, but not *parp1,2*, before and after flg22 treatment (Figure 6C), suggesting that PARG1-mediated removal of MARylation promotes polyubiquitination of SZF1, thereby destabilizing SZF1. Consistently, SZF1 protein levels were higher in *parg1* than those in WT or *parp1,2* of *pSZF1::SZF1-FLAG* transgenic plants (Figure 6D). In addition, the protein levels of $SZF1^{mDE}$, the MARylation mutant, were lower than SZF1 in multiple independent transgenic lines (Figure 6E). Furthermore, ubiquitination levels of $SZF1^{mDE}$ were higher than SZF1 in transgenic plants (Figure 6F). Collectively, our data demonstrate that flg22 treatment promotes dissociation of PARG1 from SZF1, resulting in increased SZF1 MARylation, which in turn suppresses SZF1 polyubiquitination and stabilizes SZF1 proteins.

SZF1, SZF2, and SRO2 regulate plant immunity

Both *szf1* and *szf2* mutants (Figure S6A) exhibited enhanced susceptibility to virulent bacteria *Pst* DC3000 (Figure 7A) and *P. syringae* pv. *maculicola* (*Psm*) ES4326 (Figure S6B) and nonpathogenic *Pst* DC3000 *hrcC* (Figure S6C) compared with WT plants. The *szf1,2* double mutants displayed further enhanced disease susceptibility compared with single mutants, suggesting the functional redundancy of SZF1/SZF2 in plant immunity. *Pst* DC3000-induced expression of *PR1* and *PR5* was reduced in *szf* mutants (Figures S6D and S6E). In addition, overexpression lines of *SZF1/SZF2* (Figures S6F–S6I) were more resistant to *Pst* DC3000 than WT plants (Figure S6J). The complementation of *SZF1*, but not $SZF1^{mDE}$, under its native promoter in *szf1*, restored the disease susceptibility to the WT level (Figure 7B), indicating that MARylation of SZF1 is essential for its function in plant immunity.

Flg22-induced MAPK activation and ROS burst did not show detectable differences between WT and *szf* mutants (Figures S7A and S7B). However, *szf* mutants compromised flg22-induced callose deposits and *PR1* induction (Figures 7C and S7C). SZF1, but not $SZF1^{mDE}$, restored callose deposition defects of *szf1* to the WT level (Figure S7D). In addition,

Please cite this article in press as: Kong et al., Noncanonical mono(ADP-ribosyl)ation of zinc finger SZF proteins counteracts ubiquitination for protein homeostasis in plant immunity, Molecular Cell (2021), https://doi.org/10.1016/j.molcel.2021.09.006

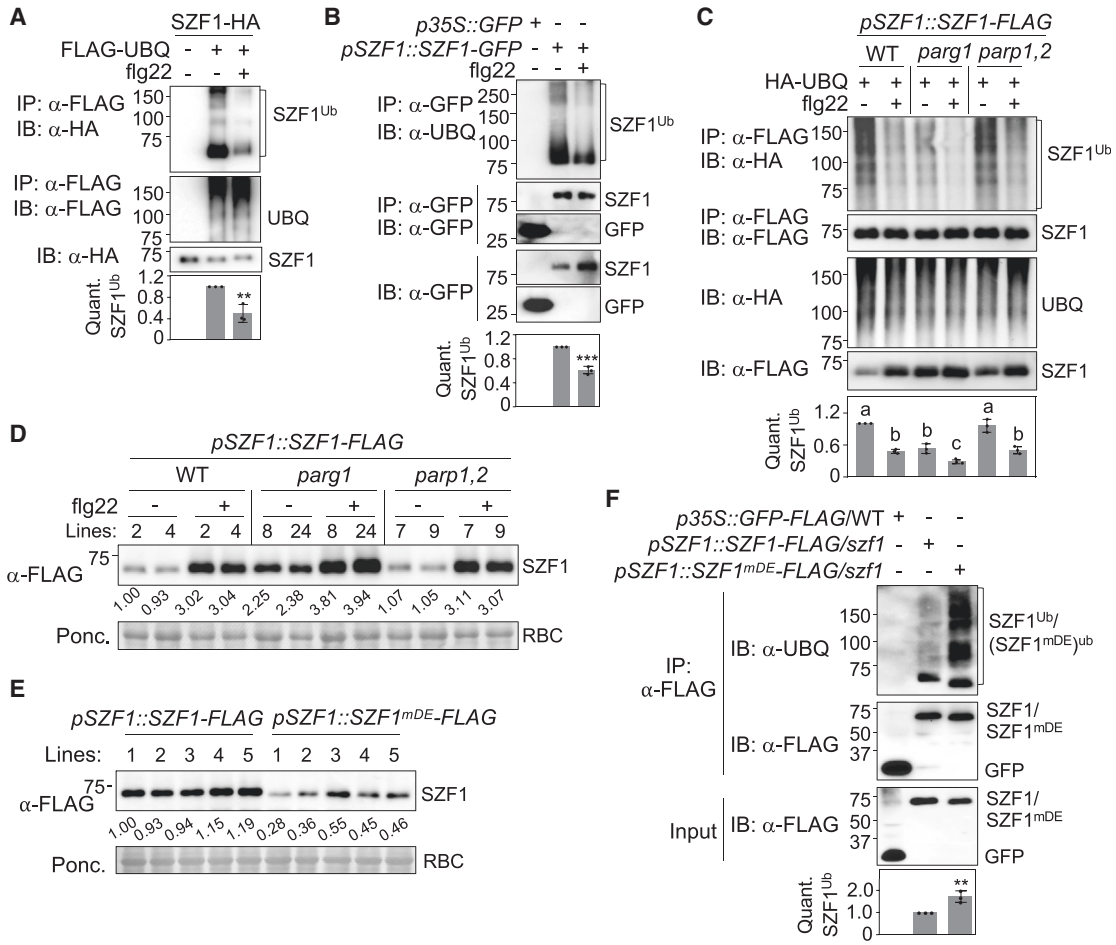

Figure 6. SZF1 MARylation regulates its ubiquitination and stability

(A) Flg22 treatment reduces SZF1 ubiquitination in protoplasts. Protoplasts expressing SZF1-HA and FLAG-UBQ were treated with 0.1 μM flg22 for 1 h, followed by coIP using α-FLAG agarose and IB using α-HA or α-FLAG antibody (top two) with input SZF1 proteins shown by α-HA IB (third).

(B) Flg22 treatment reduces SZF1 ubiquitination in *pSZF1::SZF1-GFP/szf1* transgenic plants. Ten-day-old seedlings were treated with 0.1 μM flg22 for 1 h and subjected to IP using GFP-trap beads followed by IB using α-UBQ or α-GFP antibody (top three) with input proteins shown (fourth and fifth panels).

(C) SZF1 ubiquitination is reduced in *parg1* but not *parp1,2*. Transgenic plants carrying *pSZF1::SZF1-FLAG* in WT, *parg1*, and *parp1,2* were used to express HA-UBQ in protoplasts. IP and IB were performed as in (A). SZF1 proteins were adjusted to a similar level for ubiquitination assays in (A)–(C).

(D) SZF1 proteins are stabilized in *parg1*. Ten-day-old seedlings of two representative transgenic lines of *pSZF1::SZF1-FLAG* in WT, *parg1*, and *parp1,2* were treated with or without 0.1 μM flg22 for 1 h and subjected to IB using α-FLAG antibody.

(E) Protein levels of $SZF1^{mDE}$ are lower than that of SZF1 in transgenic plants. Multiple independent transgenic lines of *pSZF1::SZF1-FLAG/szf1* and *pSZF1::$SZF1^{mDE}$-FLAG/szf1* were subjected to IB using α-FLAG antibody. Relative band intensities of SZF1 normalized to loading controls were labeled (D and E).

(F) $SZF1^{mDE}$ ubiquitination is increased in transgenic plants. Ubiquitination assay was performed as in (B) using *pSZF1::SZF1-FLAG/szf1* and *pSZF1::$SZF1^{mDE}$-FLAG/szf1* transgenic plants. *p35S::GFP-FLAG*/WT is a control. SZF1 and $SZF1^{mDE}$ proteins were adjusted to a similar level for ubiquitination assays.

Quantification of ubiquitinated SZF1 (A–C and F) is shown as an overlay of dot plot with mean ± SD; n = 3. Asterisks represent significant differences (**$p < 0.01$ and ***$p < 0.001$, Student's t test). Different letters in (C) indicate significant differences with others ($p < 0.05$, one-way ANOVA). Experiments were repeated three times with similar results.

flg22-primed plant resistance against *Pst* DC3000 was compromised in *szf* mutants compared with WT plants (Figure 7D). The redundancy of SZF1/SZF2 in flg22-primed resistance appeared not as obvious as that in basal resistance (Figure 7A). The data suggest that SZF1/SZF2 are involved in late but not early PTI responses, consistent with the functions of TZF family proteins in gene regulation (Qu et al., 2014; Tabassum et al., 2020). *Arabidopsis* PARG1, PARPs, and DDL also regulate plant late but not early PTI responses (Feng et al., 2015, 2016b). Both *sro2-1* and *sro2-2* mutants (Figure S7E) exhibited enhanced susceptibility to *Pst* DC3000 and DC3000 *hrcC* compared with WT plants (Figures 7E and S7F). Flg22-induced callose deposits were also compromised in *sro2* (Figure 7F). In addition, both *szf* and *sro2* mutants displayed enhanced disease susceptibility to avirulent *Pst* DC3000 carrying effector *avrRpt2* compared with WT plants (Figures S7G and S7H). Thus, similar to SZF1/SZF2, SRO2 regulates plant immunity against bacterial pathogens.

Please cite this article in press as: Kong et al., Noncanonical mono(ADP-ribosyl)ation of zinc finger SZF proteins counteracts ubiquitination for protein homeostasis in plant immunity, Molecular Cell (2021), https://doi.org/10.1016/j.molcel.2021.09.006

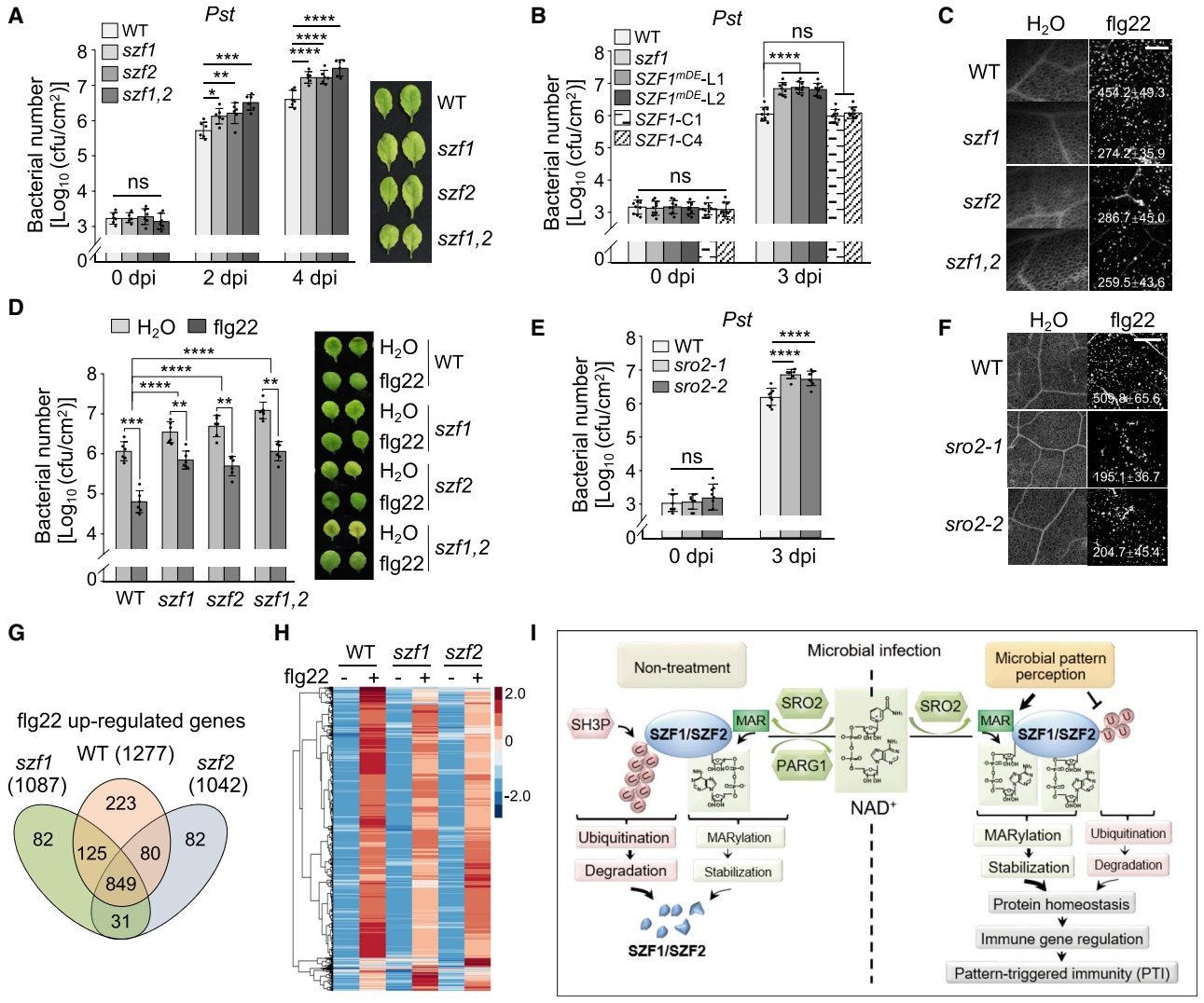

Figure 7. SZF1, SZF2, and SRO2 regulate plant immunity

(A) The *szf* mutants show increased susceptibility to *Pst* DC3000. Four-week-old plants were hand-inoculated with bacterial suspension at 5 × 10^5 cfu/mL. Bacterial growth was measured at 0, 2, and 4 days post-inoculation (dpi), and leaf pictures were taken at 4 dpi.

(B) SZF1, but not $SZF1^{mDE}$, complements *szf1* disease resistance to *Pst* DC3000. Bacterial growth was measured at 0 and 3 dpi.

(C) Flg22-triggered callose deposits are compromised in *szf* mutants. Callose deposits from 4-week-old plants were detected at 24 h after 0.5 μM flg22 treatment and visualized using a fluorescence microscope under UV light. Quantification by ImageJ is shown as mean ± SD; n = 6. Scale bar, 500 μm.

(D) Flg22-mediated immunity to *Pst* DC3000 is compromised in *szf* mutants. Leaves from 4-week-old plants were pre-infiltrated with 0.1 μM flg22 or ddH_2O for 24 h before *Pst* DC3000 inoculation. Bacterial growth was measured at 3 dpi.

(E) The *sro2* mutants show increased susceptibility to *Pst* DC3000. Assays were performed as in (A).

(F) Flg22-triggered callose deposits are reduced in *sro2* mutants. Experiments were performed as in (C).

(G) Venn diagram of flg22-upregulated genes (fold change ≥ 2 and p value < 0.05) in WT, *szf1*, and *szf2*. See Tables S4 and S5.

(H) Heatmap of flg22-induced genes in WT, *szf1*, and *szf2*. Original transcripts per million (TPM) values were subjected to data adjustment by normalized genes for generating the heatmap, with red indicating relatively high expression and blue for low expression. See Table S4.

(I) A model of SZF1 MARylation and ubiquitination in plant immunity. Without infections, SZF1 undergoes SH3P1/2-mediated polyubiquitination, leading to protein degradation. Upon microbial pattern perception, MARylation of SZF1 mediated by SRO2 is enhanced because of dissociation with PARG1, which removes MAR from SZF1. MARylation of SZF1 reduces its ubiquitination, thereby stabilizing SZF1 protein. A similar mechanism likely exists for SZF2. SZF1/SZF2 probably bind to immunity-related mRNAs and regulate their stability, contributing to plant immunity.

Data (A, B, D, and E) are shown as an overlay of dot plot with mean ± SD (A and D, n = 6; B, n = 9; E, n = 8). Asterisks represent significant differences (ns, not significant; *p < 0.05, **p < 0.01, ***p < 0.001, and ****p < 0.0001, one-way ANOVA). Experiments were repeated at least three times with similar results (G and H are based on three biological replicates). See also Figures S6 and S7 and Tables S2, S3, S4, S5, and S6.

Please cite this article in press as: Kong et al., Noncanonical mono(ADP-ribosyl)ation of zinc finger SZF proteins counteracts ubiquitination for protein homeostasis in plant immunity, Molecular Cell (2021), https://doi.org/10.1016/j.molcel.2021.09.006

SZF1/SZF2 regulate immune gene expression

RNA sequencing (RNA-seq) analysis indicated that the correlation coefficient (R) of all transcripts between WT and *szf1/szf2* without flg22 treatment was close to linear (0.94) (Figure S7I; Tables S2 and S3), indicating that SZF1/SZF2 do not profoundly affect general gene transcription. Flg22 treatment induced 1,277, 1,087, and 1,042 genes in WT, *szf1*, and *szf2*, respectively, with 849 genes overlapping in all three genotypes (Figure 7G; Table S4). Hierarchical clustering analysis of flg22-induced genes suggested that *szf1* and *szf2* mutants displayed an overall decreased flg22 response compared with WT plants (Figure 7H; Table S4). We further analyzed 623 (223 + 82 + 82 + 31 + 125 + 80) of differentially flg22-induced genes in WT, *szf1*, or *szf2* and defined them as SZF-dependent flg22-induced genes (not induced in at least one genotype) (Figure 7G; Table S5). Enrichment analysis of Gene Ontology (GO) categories of 623 genes indicated that genes related to stress, defense, immune system, bacterium, biotic stimulus, and different hormone responses were significantly enriched (Figure S7J; Table S6).

Among 623 SZF-dependent flg22-induced genes, 254 genes (223 + 31) were co-regulated by SZF1 and SZF2, whereas 369 genes (82 + 82 + 125 + 80) were specifically regulated by either SZF1 (82 + 80) or SZF2 (82 + 125) (Figure 7G; Table S5), indicating that although being close homologs, SZF1 and SZF2 may regulate different groups of genes, supporting the redundant functions of SZF1 and SZF2 in plant immunity. SZF-dependent flg22-induced genes include key immune regulatory components encoding RLKs, such as Elongation Factor-Tu Receptor (EFR), RLCKs, such as Botrytis-Induced Kinase 1 (BIK1), MAPK cascades, such as MAPK kinase 5 (MKK5), and WRKY transcription factors. Thus, SZF1/SZF2 are important regulators in controlling immune gene expression.

DISCUSSION

Plant PARPs have been genetically linked with circadian rhythm, flowering, stress responses, and immunity. We show here that plant-specific PARP-like protein SRO2, but not canonical PARPs, is a mono-ART, catalyzing the MARylation of tandem CCCH-type ZnF proteins SZF1/SZF2 in *Arabidopsis*. SZF1/SZF2 are important immune regulators, loss of which rendered plants immunocompromised. SZF1/SZF2 interact with PARG1, which removes MAR from acceptor proteins and reduces the MARylation of SZF1/SZF2. Upon MAMP treatment, PARG1 dissociates from SZF1/SZF2, resulting in the increased MARylation of SZF1/SZF2. MARylation of SZF1 counteracts the SH3 domain-containing protein SH3P1/SH3P2-mediated polyubiquitination, thereby stabilizing SZF1 (Figure 7I). We thus elucidated a mechanism of regulating protein homeostasis by the coordinated action of protein MARylation and polyubiquitination.

Among 17 human PARPs, most of them are mono-ARTs, implicating a ubiquitous presence and importance of MARylation in eukaryotes (Hottiger, 2015). To date, there were no mono-ARTs characterized in plants, even though that MARylation was hinted to exist in *Arabidopsis* (Wang et al., 2011). We uncovered that SRO2 is a mono-ART that directly catalyzes MARylation of SZF1/SZF2. Although wheat SRO protein Ta-sro1 showed PARP activities (Liu et al., 2014), plant RCD1/SROs lack the conserved NAD^+-coordinating H-Y-E motif and are considered to be noncanonical ARTs (Jaspers et al., 2010; Wirthmueller et al., 2018). However, not all human PARPs carry the H-Y-E motif. The human PARPs without the H-Y-E motif mainly mediate MARylation (Vyas et al., 2014). SRO2 without the H-Y-E motif functioning as a mono-ART further corroborates this notion.

MARylation affects target protein activity, localization, interaction, stability, and substrate specificity (Feijs et al., 2013; O'Sullivan et al., 2019). *P. syringae* effector HopF2 MARylates MKKs to inactivate their kinase activities in suppressing plant immunity (Wang et al., 2010). In contrast, *P. syringae* effector AvrRpm1 MARylates immune regulator RIN4 to promote RIN4 phosphorylation (Redditt et al., 2019). Plant mono-ART SRO2 MARylates SZF1 to stabilize SZF1 by counteracting its polyubiquitination. PARylation of a RING-domain E3 ubiquitin ligase RNF146 by human poly-ART tankyrases activates RNF146 ubiquitin ligase activity, promoting the degradation of substrate proteins (DaRosa et al., 2015). Human PARP9 is usually inactive; however, its heterodimerization with E3 ligase Dtx3L activates its mono-ART activity (Yang et al., 2017). It remains unknown how SZF1 MARylation affects its ubiquitination. MARylation may change SZF conformation, thereby reducing its accessibility to E3 ligases. Alternatively, MAR attached to SZF1 may serve as scaffolds to block its interaction with E3 ligases or recruit certain deubiquitinases to SZF1 for deubiquitination. Alternatively, MARylation at specific residues may compete with ubiquitination of nearby Lys residues.

Arabidopsis encodes 11 TZFs with functions in plant growth, hormone signaling, stress responses (Jang, 2016). Several *Arabidopsis* TZFs, such as TZF1 and TZF9, carry RNA-binding activities and localize in P-bodies, the cytoplasmic foci for mRNA storage, turnover, and sorting (Qu et al., 2014; Tabassum et al., 2020). SZF1/SZF2 also localize in P-bodies with demonstrated roles regulating mRNA turnover in plant immunity (Yu et al., 2019b). Thus, SZF1/SZF2 may regulate RNA metabolisms, such as mRNA stability and decay. SZF1/SZF2 negatively regulate salt stress by suppressing salt-responsive gene expression (Sun et al., 2007). Interestingly, SZF1/SZF2 positively regulate plant immunity by modulating a subset of flg22-induced genes. SZF1/SZF2 exert opposing roles in regulating plant immunity and salt stress. Conversely, flg22 treatment increased, whereas salt treatment reduced SZF1 protein stability. TZF9 also positively regulates plant immunity, and flg22 treatment reduces its stability (Maldonado-Bonilla et al., 2014; Tabassum et al., 2020). TZF9 is phosphorylated by MPK3/MPK6, which is essential for flg22-induced TZF9 turnover. In contrast, SZF1/SZF2 are MARylated for flg22-induced protein accumulation. Thus, differential modifications, subcellular localization, and mRNA targets may dictate distinct functions of different TZFs/SZFs in plant biological processes.

Limitations of the study

We show that ART SRO2 MARylates SZF1/SZF2, which counteracts SH3P1/SH3P2-mediated SZF1 protein ubiquitination and degradation. Although most experiments were performed in transgenic plants carrying *SZF1* under its native promoter, it requires future investigation whether the endogenous SZF1/SZF2

proteins undergo similar modifications. In addition, we identified multiple MARylation sites of SZF1/SZF2. However, as each ADP-ribose adds 0.6 kDa to a protein in molecular mass, it is ambiguous to ascertain whether multiple sites are ADP-ribosylated simultaneously or alternatively. Future development of SZF antibodies and MARylation-specific antibodies and the improved sensitivity of mass spectrometry may alleviate these limitations.

STAR★METHODS

Detailed methods are provided in the online version of this paper and include the following:

- KEY RESOURCES TABLE
- RESOURCE AVAILABILITY
  - Lead contact
  - Materials availability
  - Data and code availability
- EXPERIMENTAL MODEL AND SUBJECT DETAILS
  - Plant materials and growth conditions
  - Bacterial strains
- METHOD DETAILS
  - Constructs and transgenic plant generation
  - Generation of parp1,2,3 CRISPR/Cas lines
  - Yeast two-hybrid (Y2H) screen
  - Bacterial infection assay
  - Flg22 and chemical inhibitor treatments
  - Callose deposition
  - RNA isolation and RT-qPCR analysis
  - Co-immunoprecipitation (Co-IP) assay
  - Pull-down assay
  - ADP-ribosylation assays
  - Subcellular localization and FRET-FLIM assay
  - Agrobacterium-mediated VIGS assay
  - ROS burst assay
  - RNA sequencing analysis
  - LC-MS/MS analysis
- QUANTIFICATION AND STATISTICAL ANALYSIS

SUPPLEMENTAL INFORMATION

Supplemental information can be found online at https://doi.org/10.1016/j.molcel.2021.09.006.

ACKNOWLEDGMENTS

We thank the *Arabidopsis* Biological Resource Center (ABRC) and Dr. Chuanyou Li (Chinese Academy of Sciences) for providing *Arabidopsis* T-DNA insertion lines, Dr. Qijun Chen (China Agricultural University) for the CRISPR-Cas9 system, the proteomics core at the University of Texas Southwestern Medical Center for providing MS analysis of MARylation sites, the proteomics core at the University of Texas Medical Branch at Galveston for providing MS analysis of SZF1 interacting proteins, and the members of Drs. He and Shan laboratories for discussions. This work was supported by the National Science Foundation (NSF) (IOS-1951094) and the NIH (R01GM092893) to P.H.; the NIH (R01GM097247) to L.S.; the NSF (MCB-1906060) to J.-C.J., P.H., L.S., and Y.W.; the Wellcome Trust (101794 and 210634); the Biotechnology and Biological Sciences Research Council (BB/R007195/1); and Cancer Research UK (C35050/A22284) to I.A.

AUTHOR CONTRIBUTIONS

L.K., L.S., and P.H. conceived the study, designed experiments, and analyzed data. L.K. performed most of the molecular, biochemical, confocal microscopy, and transgenic experiments. B.F. initiated the project by identifying SZF1, performing phenotypical, molecular, and biochemical assays, and generating SZF1 transgenic plants. L.K., B.F., and L.X. performed RNA-seq analysis. Y.Y. identified *sro2* mutants and performed disease infection assays. J.H.K. characterized SZF1 stability to salt. C.Z. helped identify SZF1^{mDE} and *pSZF1:SZF1-HA/sh3p1* transgenic plants. J.-C.J., J.G.M.R., and I.A. provided the reagents. I.A., J.-C.J., and Y.W. analyzed data and provided critical feedback. L.K., L.S., and P.H. wrote the manuscript with input from all authors.

DECLARATION OF INTERESTS

The authors declare no competing interests.

Received: November 18, 2020
Revised: August 8, 2021
Accepted: September 3, 2021
Published: September 29, 2021

REFERENCES

Albert, I., Hua, C., Nürnberger, T., Pruitt, R.N., and Zhang, L. (2020). Surface sensor systems in plant immunity. Plant Physiol. *182*, 1582–1596.

Bai, P. (2015). Biology of poly(ADP-ribose) polymerases: the factotums of cell maintenance. Mol. Cell *58*, 947–958.

Briggs, A.G., and Bent, A.F. (2011). Poly(ADP-ribosyl)ation in plants. Trends Plant Sci. *16*, 372–380.

Bücherl, C., Aker, J., de Vries, S., and Borst, J.W. (2010). Probing protein-protein Interactions with FRET-FLIM. Methods Mol. Biol. *655*, 389–399.

Cohen, M.S., and Chang, P. (2018). Insights into the biogenesis, function, and regulation of ADP-ribosylation. Nat. Chem. Biol. *14*, 236–243.

Couto, D., and Zipfel, C. (2016). Regulation of pattern recognition receptor signalling in plants. Nat. Rev. Immunol. *16*, 537–552.

Daniels, C.M., Ong, S.E., and Leung, A.K. (2014). Phosphoproteomic approach to characterize protein mono- and poly(ADP-ribosyl)ation sites from cells. J. Proteome Res. *13*, 3510–3522.

DaRosa, P.A., Wang, Z., Jiang, X., Pruneda, J.N., Cong, F., Klevit, R.E., and Xu, W. (2015). Allosteric activation of the RNF146 ubiquitin ligase by a poly(ADP-ribosyl)ation signal. Nature *517*, 223–226.

de Oliveira, M.V.V., Xu, G., Li, B., de Souza Vespoli, L., Meng, X., Chen, X., Yu, X., de Souza, S.A., Intorne, A.C., de A Manhães, A.M., et al. (2016). Specific control of Arabidopsis BAK1/SERK4-regulated cell death by protein glycosylation. Nat. Plants *2*, 15218.

Escocard de Azevedo Manhães, A.M., Ortiz-Morea, F.A., He, P., and Shan, L. (2021). Plant plasma membrane-resident receptors: surveillance for infections and coordination for growth and development. J. Integr. Plant Biol. *63*, 79–101.

Feijs, K.L., Forst, A.H., Verheugd, P., and Lüscher, B. (2013). Macrodomain-containing proteins: regulating new intracellular functions of mono(ADP-ribosyl)ation. Nat. Rev. Mol. Cell Biol. *14*, 443–451.

Feng, B., Liu, C., de Oliveira, M.V., Intorne, A.C., Li, B., Babilonia, K., de Souza Filho, G.A., Shan, L., and He, P. (2015). Protein poly(ADP-ribosyl)ation regulates arabidopsis immune gene expression and defense responses. PLoS Genet. *11*, e1004936.

Feng, B., Liu, C., Shan, L., and He, P. (2016a). Protein ADP-ribosylation takes control in plant-bacterium interactions. PLoS Pathog. *12*, e1005941.

Feng, B., Ma, S., Chen, S., Zhu, N., Zhang, S., Yu, B., Yu, Y., Le, B., Chen, X., Dinesh-Kumar, S.P., et al. (2016b). PARylation of the forkhead-associated domain protein DAWDLE regulates plant immunity. EMBO Rep. *17*, 1799–1813.

Fontana, P., Bonfiglio, J.J., Palazzo, L., Bartlett, E., Matic, I., and Ahel, I. (2017). Serine ADP-ribosylation reversal by the hydrolase ARH3. eLife *6*, e28533.

He, P., Shan, L., Lin, N.C., Martin, G.B., Kemmerling, B., Nürnberger, T., and Sheen, J. (2006). Specific bacterial suppressors of MAMP signaling upstream of MAPKKK in Arabidopsis innate immunity. Cell *125*, 563–575.

Heck, A.M., and Wilusz, J. (2018). The interplay between the RNA decay and translation machinery in eukaryotes. Cold Spring Harb. Perspect. Biol. *10*, a032839.

Hottiger, M.O. (2015). SnapShot: ADP-ribosylation signaling. Mol. Cell *58*, 1134.e1.

Jang, J.C. (2016). Arginine-rich motif-tandem CCCH zinc finger proteins in plant stress responses and post-transcriptional regulation of gene expression. Plant Sci. *252*, 118–124.

Jaspers, P., Overmyer, K., Wrzaczek, M., Vainonen, J.P., Blomster, T., Salojärvi, J., Reddy, R.A., and Kangasjärvi, J. (2010). The RST and PARP-like domain containing SRO protein family: analysis of protein structure, function and conservation in land plants. BMC Genomics *11*, 170.

Jones, J.D., and Dangl, J.L. (2006). The plant immune system. Nature *444*, 323–329.

Kraus, W.L. (2020). PARPs and ADP-ribosylation: 60 years on. Genes Dev. *34*, 251–253.

Lam, B.C., Sage, T.L., Bianchi, F., and Blumwald, E. (2001). Role of SH3 domain-containing proteins in clathrin-mediated vesicle trafficking in Arabidopsis. Plant Cell *13*, 2499–2512.

Lamb, R.S., Citarelli, M., and Teotia, S. (2012). Functions of the poly(ADP-ribose) polymerase superfamily in plants. Cell. Mol. Life Sci. *69*, 175–189.

Li, F., Cheng, C., Cui, F., de Oliveira, M.V., Yu, X., Meng, X., Intorne, A.C., Babilonia, K., Li, M., Li, B., et al. (2014). Modulation of RNA polymerase II phosphorylation downstream of pathogen perception orchestrates plant immunity. Cell Host Microbe *16*, 748–758.

Li, B., Jiang, S., Yu, X., Cheng, C., Chen, S., Cheng, Y., Yuan, J.S., Jiang, D., He, P., and Shan, L. (2015). Phosphorylation of trihelix transcriptional repressor ASR3 by MAP KINASE4 negatively regulates Arabidopsis immunity. Plant Cell *27*, 839–856.

Liu, S., Liu, S., Wang, M., Wei, T., Meng, C., Wang, M., and Xia, G. (2014). A wheat SIMILAR TO RCD-ONE gene enhances seedling growth and abiotic stress resistance by modulating redox homeostasis and maintaining genomic integrity. Plant Cell *26*, 164–180.

Liu, J., Huang, Y., Kong, L., Yu, X., Feng, B., Liu, D., Zhao, B., Mendes, G.C., Yuan, P., Ge, D., et al. (2020). The malectin-like receptor-like kinase LETUM1 modulates NLR protein SUMM2 activation via MEKK2 scaffolding. Nat. Plants *6*, 1106–1115.

Love, M.I., Huber, W., and Anders, S. (2014). Moderated estimation of fold change and dispersion for RNA-seq data with DESeq2. Genome Biol. *15*, 550.

Lu, D., Lin, W., Gao, X., Wu, S., Cheng, C., Avila, J., Heese, A., Devarenne, T.P., He, P., and Shan, L. (2011). Direct ubiquitination of pattern recognition receptor FLS2 attenuates plant innate immunity. Science *332*, 1439–1442.

Maldonado-Bonilla, L.D., Eschen-Lippold, L., Gago-Zachert, S., Tabassum, N., Bauer, N., Scheel, D., and Lee, J. (2014). The Arabidopsis tandem zinc finger 9 protein binds RNA and mediates pathogen-associated molecular pattern-triggered immune responses. Plant Cell Physiol. *55*, 412–425.

Martin, M. (2011). Cutadapt removes adapter sequences from high-throughput sequencing reads. EMBnet. J. *17*, 10–12.

Nagel, M.K., Kalinowska, K., Vogel, K., Reynolds, G.D., Wu, Z., Anzenberger, F., Ichikawa, M., Tsutsumi, C., Sato, M.H., Kuster, B., et al. (2017). *Arabidopsis* SH3P2 is an ubiquitin-binding protein that functions together with ESCRT-I and the deubiquitylating enzyme AMSH3. Proc. Natl. Acad. Sci. U S A *114*, E7197–E7204.

O'Sullivan, J., Tedim Ferreira, M., Gagné, J.P., Sharma, A.K., Hendzel, M.J., Masson, J.Y., and Poirier, G.G. (2019). Emerging roles of eraser enzymes in the dynamic control of protein ADP-ribosylation. Nat. Commun. *10*, 1182.

Patro, R., Duggal, G., Love, M.I., Irizarry, R.A., and Kingsford, C. (2017). Salmon provides fast and bias-aware quantification of transcript expression. Nat. Methods *14*, 417–419.

Perina, D., Mikoč, A., Ahel, J., Ćetković, H., Žaja, R., and Ahel, I. (2014). Distribution of protein poly(ADP-ribosyl)ation systems across all domains of life. DNA Repair (Amst.) *23*, 4–16.

Qu, J., Kang, S.G., Wang, W., Musier-Forsyth, K., and Jang, J.C. (2014). The Arabidopsis thaliana tandem zinc finger 1 (AtTZF1) protein in RNA binding and decay. Plant J. *78*, 452–467.

Rack, J.G.M., Palazzo, L., and Ahel, I. (2020). (ADP-ribosyl)hydrolases: structure, function, and biology. Genes Dev. *34*, 263–284.

Redditt, T.J., Chung, E.H., Karimi, H.Z., Rodibaugh, N., Zhang, Y., Trinidad, J.C., Kim, J.H., Zhou, Q., Shen, M., Dangl, J.L., et al. (2019). AvrRpm1 functions as an ADP-ribosyl transferase to modify NOI domain-containing proteins, including arabidopsis and soybean RPM1-interacting protein4. Plant Cell *31*, 2664–2681.

Rissel, D., Losch, J., and Peiter, E. (2014). The nuclear protein Poly(ADP-ribose) polymerase 3 (AtPARP3) is required for seed storability in Arabidopsis thaliana. Plant Biol. *16*, 1058–1064.

Rosenthal, F., Feijs, K.L., Frugier, E., Bonalli, M., Forst, A.H., Imhof, R., Winkler, H.C., Fischer, D., Caflisch, A., Hassa, P.O., et al. (2013). Macrodomain-containing proteins are new mono-ADP-ribosylhydrolases. Nat. Struct. Mol. Biol. *20*, 502–507.

Shan, L., He, P., Li, J., Heese, A., Peck, S.C., Nürnberger, T., Martin, G.B., and Sheen, J. (2008). Bacterial effectors target the common signaling partner BAK1 to disrupt multiple MAMP receptor-signaling complexes and impede plant immunity. Cell Host Microbe *4*, 17–27.

Soneson, C., Love, M.I., and Robinson, M.D. (2015). Differential analyses for RNA-seq: transcript-level estimates improve gene-level inferences. F1000Res. *4*, 1521.

Song, J., Keppler, B.D., Wise, R.R., and Bent, A.F. (2015). PARP2 is the predominant poly(ADP-ribose) polymerase in Arabidopsis DNA damage and immune responses. PLoS Genet. *11*, e1005200.

Stamenova, S.D., French, M.E., He, Y., Francis, S.A., Kramer, Z.B., and Hicke, L. (2007). Ubiquitin binds to and regulates a subset of SH3 domains. Mol. Cell *25*, 273–284.

Sun, J., Jiang, H., Xu, Y., Li, H., Wu, X., Xie, Q., and Li, C. (2007). The CCCH-type zinc finger proteins AtSZF1 and AtSZF2 regulate salt stress responses in Arabidopsis. Plant Cell Physiol. *48*, 1148–1158.

Tabassum, N., Eschen-Lippold, L., Athmer, B., Baruah, M., Brode, M., Maldonado-Bonilla, L.D., Hoehenwarter, W., Hause, G., Scheel, D., and Lee, J. (2020). Phosphorylation-dependent control of an RNA granule-localized protein that fine-tunes defence gene expression at a post-transcriptional level. Plant J. *101*, 1023–1039.

Vainonen, J., Shapiguzov, A., Krasensky-Wrzaczek, J., Gossens, R., Masi, R., Danciu, I., Puukko, T., Battchikova, N., Jonak, C., Wirthmueller, L., et al. (2021). Arabidopsis poly(ADP-ribose)-binding protein RCD1 interacts with photoregulatory protein kinases in nuclear bodies. bioRxiv. https://doi.org/10.1101/2020.07.02.184937.

Vyas, S., Matic, I., Uchima, L., Rood, J., Zaja, R., Hay, R.T., Ahel, I., and Chang, P. (2014). Family-wide analysis of poly(ADP-ribose) polymerase activity. Nat. Commun. *5*, 4426.

Wang, Y., Li, J., Hou, S., Wang, X., Li, Y., Ren, D., Chen, S., Tang, X., and Zhou, J.M. (2010). A Pseudomonas syringae ADP-ribosyltransferase inhibits Arabidopsis mitogen-activated protein kinase kinases. Plant Cell *22*, 2033–2044.

Wang, H., Liang, Q., Cao, K., and Ge, X. (2011). Endogenous protein mono-ADP-ribosylation in Arabidopsis thaliana. Planta *233*, 1287–1292.

Wang, Z.P., Xing, H.L., Dong, L., Zhang, H.Y., Han, C.Y., Wang, X.C., and Chen, Q.J. (2015). Egg cell-specific promoter-controlled CRISPR/Cas9 efficiently generates homozygous mutants for multiple target genes in Arabidopsis in a single generation. Genome Biol. *16*, 144.

Wirthmueller, L., Asai, S., Rallapalli, G., Sklenar, J., Fabro, G., Kim, D.S., Lintermann, R., Jaspers, P., Wrzaczek, M., Kangasjärvi, J., et al. (2018). Arabidopsis downy mildew effector HaRxL106 suppresses plant immunity by binding to radical-induced cell death1. New Phytol. *220*, 232–248.

Wu, S., Lu, D., Kabbage, M., Wei, H.L., Swingle, B., Records, A.R., Dickman, M., He, P., and Shan, L. (2011). Bacterial effector HopF2 suppresses Arabidopsis innate immunity at the plasma membrane. Mol. Plant Microbe Interact. *24*, 585–593.

Xing, H.L., Dong, L., Wang, Z.P., Zhang, H.Y., Han, C.Y., Liu, B., Wang, X.C., and Chen, Q.J. (2014). A CRISPR/Cas9 toolkit for multiplex genome editing in plants. BMC Plant Biol. *14*, 327.

Yang, C.S., Jividen, K., Spencer, A., Dworak, N., Ni, L., Oostdyk, L.T., Chatterjee, M., Kuśmider, B., Reon, B., Parlak, M., et al. (2017). Ubiquitin modification by the E3 ligase/ADP-ribosyltransferase Dtx3L/Parp9. Mol. Cell *66*, 503–516.e5.

Yu, X., Feng, B., He, P., and Shan, L. (2017). From chaos to harmony: responses and signaling upon microbial pattern recognition. Annu. Rev. Phytopathol. *55*, 109–137.

Yu, X., Li, B., Jang, G.J., Jiang, S., Jiang, D., Jang, J.C., Wu, S.H., Shan, L., and He, P. (2019a). Orchestration of processing body dynamics and mRNA decay in Arabidopsis immunity. Cell Rep. *28*, 2194–2205.e6.

Yu, X., Xu, G., Li, B., de Souza Vespoli, L., Liu, H., Moeder, W., Chen, S., de Oliveira, M.V.V., Ariádina de Souza, S., Shao, W., et al. (2019b). The receptor kinases BAK1/SERK4 regulate Ca^{2+} channel-mediated cellular homeostasis for cell death containment. Curr. Biol. *29*, 3778–3790.e8.

Zhang, H., Gu, Z., Wu, Q., Yang, L., Liu, C., Ma, H., Xia, Y., and Ge, X. (2015). Arabidopsis PARG1 is the key factor promoting cell survival among the enzymes regulating post-translational poly(ADP-ribosyl)ation. Sci. Rep. *5*, 15892.

Zhang, J., Coaker, G., Zhou, J.M., and Dong, X. (2020). Plant immune mechanisms: from reductionistic to holistic points of view. Mol. Plant *13*, 1358–1378.

Zhou, J.M., and Zhang, Y. (2020). Plant immunity: danger perception and signaling. Cell *181*, 978–989.

Please cite this article in press as: Kong et al., Noncanonical mono(ADP-ribosyl)ation of zinc finger SZF proteins counteracts ubiquitination for protein homeostasis in plant immunity, Molecular Cell (2021), https://doi.org/10.1016/j.molcel.2021.09.006

CellPress

STAR★METHODS

KEY RESOURCES TABLE

REAGENT or RESOURCE	SOURCE	IDENTIFIER
Antibodies		
Rat monoclonal anti-HA-Peroxidase	Roche	Cat#12013819001; RRID: AB_390917
Anti-MYC-Peroxidase	MilliporeSigma	Cat#A5598; RRID: AB_439682
Mouse monoclonal anti-FLAG-Peroxidase	MilliporeSigma	Cat#A8592; RRID: AB_439702
Mouse monoclonal anti-GFP	Roche	Cat#11814460001; RRID: AB_390913
Mouse monoclonal anti-HIS-Peroxidase	Roche	Cat#11965085001; RRID: AB_514487
Mouse monoclonal anti-GST-Peroxidase	MilliporeSigma	Cat#16-209; RRID: AB_310805
Rat monoclonal anti-MBP	Biolegend	Cat#906901, RRID: AB_2565070
Rabbit polyclonal anti-UBQ11	Agrisera	Cat#AS08 307; RRID: AB_2256904
Rabbit polyclonal anti-pERK1/2	Cell Signaling	Cat#9101; RRID: AB_331646
Anti-mouse IgG HRP-linked antibody	Cell Signaling	Cat#7076; RRID: AB_330924
Anti-rabbit IgG HRP-linked antibody	Cell Signaling	Cat#7074; RRID: AB_2099233
Anti-rat IgG HRP-linked antibody	Cell Signaling	Cat#7077; RRID: AB_10694715
Bacterial and virus strains		
Escherichia coli MC1061	Yu et al., 2019b	N/A
Agrobacterium tumefaciens GV3101	Yu et al., 2019b	N/A
Yeast AH109	Li et al., 2015	N/A
E. coli BL21	Yu et al., 2019b	N/A
Pseudomonas syringae pv. *tomato* DC3000 (*Pst*)	He et al., 2006	N/A
P. syringae pv. *maculicola* ES4326 (*Psm*)	Li et al., 2015	N/A
Pseudomonas syringae pv. *tomato* DC3000 (*Pst*) type III secretion mutant *hrcC*	He et al., 2006	N/A
Pst carrying avrRpt2	Li et al., 2015	N/A
Chemicals, peptides, and recombinant proteins		
MG132	AG Scientific	Cat#99533-80-9
RiboZol RNA Extraction Reagent	AMRESCO	Cat#N580
RNase-free DNase I	NEB	Cat#M0303L
IPTG	MilliporeSigma	Cat#I6758
GelCode Blue Stain Reagent	ThermoFisher	Cat#24590
Aniline blue	MilliporeSigma	Cat#415049
Biotin-NAD^+	R&D Systems	Cat#6573
^{32}P-NAD^+	Perkin Elmer	Cat#BLU023X000MC
Ponceau S staining	MilliporeSigma	Cat#P7170
Protease Inhibitor Cocktail	Roche	Cat#12352200
Anti-FLAG M2 Affinity gel	MilliporeSigma	Cat#A2220
Anti-HA magnetic beads	ThermoFisher	Cat#88837
GFP-Trap agarose beads	Chromotek	Cat#gta-20
HRP-Conjugated Streptavidin	ThermoFisher	Cat#21130
Pierce glutathione agarose	ThermoFisher	Cat#16101
Amylose resin	NEB	Cat#E8021L
HisPur Ni-NTA Resin	ThermoFisher	Cat#88222
Af1521 Macrodomain (PAR/MAR) Affinity Resins	Tulip Biolabs	Cat#2302
PARP14m3 Magnetic Affinity Resin	Tulip Biolabs	Cat#2414
flg22	Genscript Biotech	N/A

(*Continued on next page*)

Please cite this article in press as: Kong et al., Noncanonical mono(ADP-ribosyl)ation of zinc finger SZF proteins counteracts ubiquitination for protein homeostasis in plant immunity, Molecular Cell (2021), https://doi.org/10.1016/j.molcel.2021.09.006

Continued

REAGENT or RESOURCE	SOURCE	IDENTIFIER
Critical commercial assays		
M-MuLV Reverse Transcriptase	NEB	Cat#M0253L
iTaq SYBR green Supermix	Bio-Rad	Cat#1725124
ClonExpress II one Step Cloning Kit	Vazyme	Cat#C112-02
Deposited data		
RNA-seq raw data	NCBI	PRJNA749854
Source data and unprocessed images	Mendeley Data	https://doi.org/10.17632/ffgp4cm5x3.1
Experimental models: Organisms/strains		
Arabidopsis thaliana Col-0 wild-type	Li et al., 2015	N/A
szf1	Sun et al., 2007	SALK_141550
szf2	Sun et al., 2007	SALK_024800C
szf1,2	Sun et al., 2007	N/A
parp3	ABRC	SALK_0108092
sh3p1	ABRC	SALK_116715
sro2-1	ABRC	SALK_030045
sro2-2	ABRC	CS816777/SAIL_361_A07
parg1	Feng et al., 2015	N/A
parp1,2	Feng et al., 2015	N/A
parp1,2,3 CRISPR line	This paper	N/A
p35S::GFP-FLAG/Col-0	This paper	N/A
p35S::SZF1-GFP/Col-0	This paper	N/A
p35S::SZF2-GFP/Col-0	This paper	N/A
p35S::SZF1-FLAG/Col-0	This paper	N/A
p35S::SZF2-FLAG/Col-0	This paper	N/A
pSZF1::SZF1-GFP/szf1	This paper	N/A
pSZF1::SZF1-FLAG/szf1	This paper	N/A
pSZF1::SZF1-FLAG/Col-0	This paper	N/A
pSZF1::SZF1-FLAG/sro2-1	This paper	N/A
pSZF1::SZF1-FLAG/parg1	This paper	N/A
pSZF1::SZF1-FLAG/parp1,2	This paper	N/A
pSZF1::SZF1^{mDE}-FLAG/szf1	This paper	N/A
pSZF1::SZF1-HA/Col-0	This paper	N/A
pSZF1::SZF1-HA/szf1	This paper	N/A
pSZF1::SZF1-HA/sh3p1	This paper	N/A
pSZF1::SZF1-FLAG/p35S::PARG1-HA	This paper	N/A
pSZF1::SZF1-FLAG/p35S::SH3P1-HA	This paper	N/A
pSZF1::SZF1-HA/p35S::SRO2-FLAG	This paper	N/A
pSZF1::SZF2-HA/p35S::SRO2-FLAG	This paper	N/A
Oligonucleotides		
Primers for cloning, point mutation and VIGS, see Table S7	This paper	N/A
Primers for genotyping and qRT-PCR, see Table S7	This paper	N/A
Recombinant DNA		
pYL156 (*pTRV-RNA2*)	Yu et al., 2019b	N/A
pTRV-RNA1	Yu et al., 2019b	N/A
pYL156-GFP	Yu et al., 2019b	N/A
pHBT	He et al., 2006	N/A

(*Continued on next page*)

Please cite this article in press as: Kong et al., Noncanonical mono(ADP-ribosyl)ation of zinc finger SZF proteins counteracts ubiquitination for protein homeostasis in plant immunity, Molecular Cell (2021), https://doi.org/10.1016/j.molcel.2021.09.006

Continued

REAGENT or RESOURCE	SOURCE	IDENTIFIER
pGST	Yu et al., 2019b	N/A
pCB302	Li et al., 2015	N/A
pGADT7 (AD)	Shan et al., 2008	N/A
pGBKT7 (BD)	Shan et al., 2008	N/A
pHEE401E	Xing et al., 2014	N/A
pGADT7-SZF1	This paper	N/A
pGADT7-avrPto	He et al., 2006	N/A
pGBKT7-PARG1	This paper	N/A
pGBKT7-Pto	He et al., 2006	N/A
pYL156-SH3P1	This paper	N/A
pYL156-SH3P2	This paper	N/A
pYL156-PUB2	This paper	N/A
pYL156-MAC3A	This paper	N/A
pYL156-MAC3B	This paper	N/A
pHBT-SZF1-GFP	This paper	N/A
pHBT-GFP-FLAG	This paper	N/A
pHBT-mCherry-HA	This paper	N/A
pHBT-HopF2-HA	Wu et al., 2011	N/A
pHBT-SZF1-HA	This paper	N/A
pHBT-SZF1-FLAG	This paper	N/A
pHBT-SZF1^{C}-FLAG	This paper	N/A
pHBT-SZF1^{N}-FLAG	This paper	N/A
pHBT-SZF1$^{C\Delta ZnF}$-FLAG	This paper	N/A
pHBT-SZF1^{mDE}-FLAG	This paper	N/A
pHBT-SZF2-GFP	This paper	N/A
pHBT-SZF2-FLAG	This paper	N/A
pHBT-PARG1-HA	Feng et al., 2015	N/A
pHBT-PARP2-FLAG	Feng et al., 2015	N/A
pHBT-PARP2-HA	Feng et al., 2015	N/A
pHBT-PARG1-HA	Feng et al., 2015	N/A
pHBT-PARG1-FLAG	Feng et al., 2015	N/A
pHBT-PARG1-GFP	This paper	N/A
pHBT-DDL-mCherry	This paper	N/A
pHBT-DDL-FLAG	Feng et al., 2016b	N/A
pHBT-BIR2-mCherry	Liu et al., 2020	N/A
pHBT-BAK1-GFP	Liu et al., 2020	N/A
pHBT-PARG1-mCherry	This paper	N/A
pHBT-DCP1-mCherry	Yu et al., 2019a	N/A
pHBT-NLS-RFP	Li et al., 2015	N/A
pHBT-HsMacroD2-HA	This paper	N/A
pHBT-RCD1-FLAG	This paper	N/A
pHBT-SRO2-3xFLAG	This paper	N/A
pHBT-SRO5-FLAG	This paper	N/A
pHBT-SH3P1-FLAG	This paper	N/A
pHBT-FLAG-UBQ	Lu et al., 2011	N/A
pHBT-HA-UBQ	Liu et al., 2020	N/A
pCAMBIA1300-p35S::GFP-FLAG	This paper	N/A
pCAMBIA1300-pSZF1::SZF1-FLAG	This paper	N/A

(*Continued on next page*)

Please cite this article in press as: Kong et al., Noncanonical mono(ADP-ribosyl)ation of zinc finger SZF proteins counteracts ubiquitination for protein homeostasis in plant immunity, Molecular Cell (2021), https://doi.org/10.1016/j.molcel.2021.09.006

Continued

REAGENT or RESOURCE	SOURCE	IDENTIFIER
pCAMBIA1300-pSZF1::SZF1^{mDE}-FLAG	This paper	N/A
pCAMBIA1300-pSZF1::SZF1-HA	This paper	N/A
pCAMBIA1300-pSZF2::SZF2-HA	This paper	N/A
pCAMBIA2300-p35S::PARG1-HA	Feng et al., 2015	N/A
pMDC32-p35S::SZF1-FLAG	This paper	N/A
pMDC32-p35S::SZF2-FLAG	This paper	N/A
pCB302-p35S::SRO2-3xFLAG	This paper	N/A
pCB302-p35S::SH3P1-HA	This paper	N/A
pGST-SZF1	This paper	N/A
pGST-SZF2	This paper	N/A
pGST-MBP	This paper	N/A
pGST-PARG1	Feng et al., 2015	N/A
pET28a-PARG1	Feng et al., 2015	N/A
pET28a-HsPARG	Feng et al., 2015	N/A
pGST-HopF2	Wu et al., 2011	N/A
pET32a-SZF2	This paper	N/A
pET32a-SZF1	This paper	N/A
pET28a-HIS-SRO2	This paper	N/A
pET28a-HIS-DDL	Feng et al., 2016b	N/A
pMAL-MBP-PARP2	Feng et al., 2015	N/A
pDEST17-HsMacroD2	Fontana et al., 2017	N/A
pDEST17-HsARH3	Fontana et al., 2017	N/A
Software and algorithms		
ImageJ	NIH	https://imagej.nih.gov/ij/
GraphPad prism 8	GraphPad	https://www.graphpad.com/scientific-software/prism/
Photoshop CS6	Adobe	https://www.adobe.com/

RESOURCE AVAILABILITY

Lead contact

Further information and requests for resources should be directed to and will be fulfilled by the Lead Contact, Ping He (pinghe@tamu.edu).

Materials availability

We will distribute the plasmids and transgenic plants freely to the scientific community upon request.

Data and code availability

- Raw RNA-seq data have been deposited at National Center for Biotechnology Information (NCBI) and are publicly available as of the date of publication. Accession number is listed in the key resources table. Original western blot images, and source data-sets have been deposited at Mendeley Data and are publicly available as of the date of publication. The DOI is listed in the key resources table.
- This paper does not report original code.
- Any additional information required to reanalyze the data reported in this paper is available from the lead contact upon request.

EXPERIMENTAL MODEL AND SUBJECT DETAILS

Plant materials and growth conditions

Arabidopsis thaliana T-DNA insertion lines szf1 (SALK_141550), szf2 (SALK_024800C), parp3 (SALK_0108092), sh3p1 (SALK_116715), sro2-1 (SALK_030045), and sro2-2 (CS816777/SAIL_361_A07) in the Col-0 background were obtained from

Arabidopsis Biological Resource Center (ABRC), and the homozygous lines were identified using the genomic PCR. The szf1,2 homozygous double mutant lines were reported previously (Sun et al., 2007). The parg1 and parp1,2 double mutants were reported in our previous study (Feng et al., 2015). Various mutants and transgenic lines used in this study were described in the Key Resources Table.

All *A. thaliana* and *Nicotiana benthamiana* plants were grown on soil (Metro Mix 366) in a growth room at 23°C, 50% relative humidity, and 75-100 $\mu Em^{-2}s^{-1}$ light with a 12-hr light/12-hr dark photoperiod for 4-5 weeks for protoplast isolation, ROS production, and disease assays. Seedlings were germinated on plates containing half-strength Murashige and Skoog medium (½MS) with 0.5% sucrose, 0.8% agar, and 2.5 mM MES at pH 5.7, and grown under the same condition as above for 10-14 days for protein stability assays, RT-qPCR, and RNA-Seq analysis.

Bacterial strains

The bacterial and yeast strains used in this study include *Agrobacterium tumefaciens* GV3101, *Escherichia coli* MC1061 and BL21, *Saccharomyces cerevisiae* AH109, *Pseudomonas syringae* pv. *tomato* DC3000 (*Pst*), *Pst hrcC*, and *P. syringae* pv. *maculicola* ES4326 (*Psm*). *Pst*, *Pst avrRpt2,* and *Pst hrcC* were grown on the King's B medium plates with 50 μg/mL rifamycin, and *Psm* was grown with 50 μg/mL streptomycin. All the *Pseudomonas* strains and *Agrobacterium* strains were incubated at 28°C for 2-3 days before culturing in the liquid medium. All the *E. coli* strains were incubated at 37°C for 1 day for different experiments. The yeast AH109 was incubated at 30°C for 3 days for yeast two-hybrid (Y2H) experiments.

METHOD DETAILS

Constructs and transgenic plant generation

The pHBT-PARP2-3xFLAG, pHBT-PARP2-HA, pMAL-PARP2, pHBT-PARG1-FLAG, pHBT-PARG1-HA, pHBT-PARG1-GFP, pGEX4T-PARG1, pET28a-PARG1, pDEST17-HsMacroD2, pDEST17-HsARH3, and pDEST17-HsPARG constructs were reported previously (Feng et al., 2015; Fontana et al., 2017). cDNA of SZF1, SZF2, SRO5, and SH3P1 was amplified from Col-0 cDNA with primers containing BamHI at the 5′-terminus and StuI at the 3′-terminus (Table S7), and ligated into a plant protoplast expression vector pHBT under the control of a CaMV 35S promoter with the FLAG, HA or GFP epitope tag at the C terminus. PARG1, DDL, and BIR2 were subcloned into pHBT with the mCherry tag at the C terminus using BamHI and SmaI digestion. The SZF1 truncation mutants and MARylation site mutants were cloned using the full-length SZF1 constructs as the template and primers, as listed in Table S7. The cDNA of RCD1 and SRO2 was amplified from Col-0 cDNA and ligated into pHBT vectors with FLAG or HA tag using the ClonExpress II one Step Cloning Kit (Vazyme) according to the manufacture protocols. Human HsMacroD2 in pDEST17 vector were sub-cloned into pHBT vector using the ClonExpress II one Step Cloning Kit. The SZF1, SZF2, and PARG1 in pHBT vector were subcloned into pGADT7 (AD) and pGBKT7 (BD, Clontech) for yeast two-hybrid (Y2H) assays using BamHI or NcoI and StuI digestion. Meanwhile, SZF1 and SZF2 in pHBT vectors were sub-cloned into binary vectors pCAMBIA1300 (1x35S promoter) and pMDC32 (2x35S promoter) using BamHI and StuI digestion.

To generate *E. coli* fusion protein expression vectors, *SZF1*, *SZF2*, and SRO2 in *pHBT* vector were subcloned into a modified GST or HIS fusion protein expression vector *pGEX4T-1* (Pharmacia) and *pET28a-SUMO* using BamHI or BglII and StuI digestion.

To construct the native promoter-driven *SZF1* and *SZF2* in the *pCAMBIA1300* binary vector for *Agrobacterium*-mediated transformation, the *SZF1* or *SZF2* promoter (~2 kb upstream of the start codon) was amplified from Col-0 genomic DNA using primers containing XbaI at the 5′-terminus and BamHI at the 3′-terminus and was used to replace the *35S* promoter in the *pCAMBIA1300* vector to obtain the p*CAMBIA1300-pSZF1::SZF1-FLAG* and *pCAMBIA1300-pSZF2::SZF2-FLAG* binary vectors, respectively. The *SRO2* cDNA was amplified from *pHBT* vector and subcloned to *pCB302* vector under the *35S* promoter using NcoI and StuI digestion. These binary constructs were transformed into *A. tumefaciens* strain GV3101 for generating transgenic plants using the floral dipping method.

To construct the *pYL156* vectors for virus-induced gene silencing (VIGS) assay, a ~500 bp coding region fragment of the indicated genes (*SH3P1*, *SH3P2*, *PUB2*, *MAC3A,* and *MAC3B*) without predicted off-targets was designed via the Solanaceae Genomics Network (https://solgenomics.net) and was amplified from Col-0 cDNA with primers containing EcoRI at the 5′-terminus and KpnI at the 3′-terminus (Table S7). The PCR fragments were ligated into VIGS vector *pYL156* after digestion with EcoRI and KpnI.

All primers used in this study were listed in Table S7, and the Sanger-sequencing verified all insertions in different vectors.

Generation of parp1,2,3 CRISPR/Cas lines

The *parp1,2,3* triple mutant was generated by the CRISPR–Cas9 system following the published protocol (Wang et al., 2015; Yu et al., 2019b). Briefly, primers containing guide RNA (gRNA) sequences of *PARP1* and *PARP2* were used in PCR to insert both *gRNA* sequences into the *pDT1T2* vector. The *pDT1T2* vector containing both *gRNAs* was further PCR amplified, and the PCR products were digested with BsaI and ligated into the binary vector *pHEE401E*. The *pHEE401* containing two gRNA of *PARP1* and *PARP2* was transformed into *parp3* T-DNA insertion mutant plants using the *Agrobacterium*-mediated floral dip method. Genomic DNAs from hygromycin (50 μg/mL) positive plants were extracted, PCR amplified with gene-specific primers, and sequenced by Sanger sequencing to identify *parp1,2,3* mutants. The primers were list in Table S7.

Please cite this article in press as: Kong et al., Noncanonical mono(ADP-ribosyl)ation of zinc finger SZF proteins counteracts ubiquitination for protein homeostasis in plant immunity, Molecular Cell (2021), https://doi.org/10.1016/j.molcel.2021.09.006

Yeast two-hybrid (Y2H) screen

The *Arabidopsis* cDNA library constructed in a modified *pGADT7* vector (Clontech) was previously described (Lu et al., 2011). *PARG1* from *pHBT-PARG1-HA* was sub-cloned into a modified *pGBKT7* vector with NcoI and StuI digestion and transformed into the yeast AH109 strain. The resulting yeast transformant was then transformed with the *Arabidopsis* cDNA library and screened in the synthetic defined media (SD) without Trp, Leu, His, Ade (SD-TLHA), and SD-TLH containing 1 mM 3-amino-1, 2, 4-triazole (3-AT). The confirmed yeast colonies were subjected to plasmid isolation and sequencing.

Bacterial infection assay

Pst, *Psm*, and *hrcC* were cultured in the King's B medium supplemented with 2 mM $MgSO_4$ and the appropriate antibiotics (50 μg/mL streptomycin, rifampicin, or kanamycin) at 28°C for overnight. Bacteria were harvested by centrifugation at 2500 g for 5 min, washed twice with ddH_2O, and adjusted to the desired concentration with 10 mM $MgCl_2$. Leaves of four-week-old *Arabidopsis* plants were hand-infiltrated with bacterial suspension using a 1-mL needleless syringe and collected at the indicated times for bacterial growth assays. To measure bacterial growth, two leaf discs were ground in 100 mL H_2O, and serial dilutions were plated on TSA medium (1% Bacto tryptone, 1% sucrose, 0.1% glutamic acid, 1.5% agar) containing the appropriate antibiotics. Bacterial colony-forming units (cfu) were counted at zero, two, or three days after inoculation (dpi).

Flg22 and chemical inhibitor treatments

The concentration of flg22 used in this study is 0.1 μM (for the treatment of protoplasts and seedlings) and 0.5 μM (for callose deposition assay). For the seedling treatments, the concentration of MG132 (AG Scientific #99533-80-9) is 2 μM.

Callose deposition

Arabidopsis leaves of five-week-old soil-grown plants were hand-inoculated with 0.5 μM flg22 or ddH_2O for 12-24 hr. The leaves were collected and transferred into FAA solution (10% formaldehyde, 5% acetic acid, and 50% ethanol) for 12 hr, de-stained in 95% ethanol for 6 hr, washed twice with ddH_2O, and incubated in 0.01%–0.05% aniline blue solution (150 mM KH_2PO4, pH 9.5) for 1 hr. The callose deposits were visualized with a fluorescence microscope and were counted using ImageJ software (https://rsb.info.nih.gov/ij/).

RNA isolation and RT-qPCR analysis

Total RNA was isolated from ten-day-old seedlings grown on ½ MS plates or leaves of four-week-old plants grown in the soil after flg22 or *Pst* treatment using TRIzol reagent (Life Technologies) and quantified with NanoDrop (Thermo Scientific). The total RNA of 1 μg was treated with RNase-free DNase I (Promega) and then was reverse transcribed to synthesize the first-strand cDNA with M-MuLV reverse transcriptase (NEB) and oligo (dT) primer. The quantitative RT-PCR (RT-qPCR) was performed using iTaq SYBR green Supermix (Bio-Rad) in a Bio-Rad CFX384 Real-Time PCR System (Bio-Rad). *UBQ10* was used as an internal control. All the primers were listed in Table S7.

Co-immunoprecipitation (Co-IP) assay

Arabidopsis protoplasts transfected with the indicated constructs (empty vector as the negative control) were incubated at room temperature for 12 hr and treated with or without flg22 for the indicated time. Protoplasts were collected by centrifugation. Samples were lysed with Co-IP buffer (20 mM HEPES, pH7.5, 100 mM NaCl, 1 mM EDTA, 10% Glycerol, 0.5% Triton X-100, 2 mM NaF, 2 mM Na_3VO_4, 1 mM DTT and protease inhibitor cocktail from MilliporeSigma) by vortexing. Protein extracts were incubated with α-FLAG or α-HA agarose beads for 1-3 hr at 4°C with gentle shaking on a rocker. The beads were collected and washed three to five times with washing buffer (20 mM HEPES, pH7.5, 100 mM NaCl, 1 mM EDTA, 10% Glycerol, 0.1% Triton X-100, 2 mM NaF, 2 mM Na_3VO_4, 1 mM DTT). Immunoblots were analyzed with α-FLAG-HRP, α-HA-HRP, α-MYC-HRP, or α-GFP antibodies described in the Key Resources Table.

Pull-down assay

The fusion proteins were induced in *E. coli* BL21 strain using LB medium (1% tryptone, 0.5% yeast extracts, 1% NaCl) supplemented with 0.25 mM Isopropyl β-D-1-thiogalactopyranoside (IPTG) at 16°C for 12-18 hr. Recombinant GST-SZF1, GST-SZF2, GST-PARG1, and GST-MBP proteins were purified with Pierce glutathione agarose beads (Thermo Scientific), and MBP-PARP2 proteins were purified using amylose resin (NEB) according to the manufacture protocols. HIS-PARG1, HIS-SZF1, HIS-SZF2, HIS-HsMacroD2, HIS-HsARH3, and HIS-HsPARG proteins were purified using Pierce Ni-NTA agarose beads (Thermo Scientific) according to the manufacture protocols. GST or GST-PARG1 proteins were pre-incubated with pre-washed glutathione agarose beads in 300 μL incubation buffer (20 mM Tris-HCl, pH7.5, 100 mM NaCl, 0.1 mM EDTA and 0.5% Triton X-100) at 4°C for 1 hr. The immobilized GST-PARG1 beads were washed twice with washing buffer (20 mM Tris-HCl, pH7.5, 300 mM NaCl, 0.1mM EDTA, and 0.1% Triton X-100), and then incubated with prewashed HIS-SZF1 or HIS-SZF2 proteins for another 1 hr. The beads were collected and washed three to five times with washing buffer. Immunoblots were analyzed with an α-GST-HRP, α-HIS-HRP, or α-MBP antibodies described in the Key Resources Table.

Please cite this article in press as: Kong et al., Noncanonical mono(ADP-ribosyl)ation of zinc finger SZF proteins counteracts ubiquitination for protein homeostasis in plant immunity, Molecular Cell (2021), https://doi.org/10.1016/j.molcel.2021.09.006

ADP-ribosylation assays

The *in vitro* and *in vivo* ADP-ribosylation assays were performed as described previously (Feng et al., 2015). Briefly, for *in vivo* ADP-ribosylation assay, 1 mL of protoplasts at 2-3 × 10^5 cells mL^{-1} expressing SZF1-FLAG or SZF2-FLAG were collected by brief centrifugation and re-suspended in 100 μL WI solution (0.5 M mannitol, 20 mM KCl, 4 mM MES, pH5.7) with 1 μCi ^{32}P-NAD$^+$ pre-treatment for 1 hr followed by 0.1 μM flg22 treatment for another 1 hr. Proteins were extracted by IP buffer and subjected for immunoprecipitation assays with α-FLAG agarose beads. The immunoprecipitated proteins were separated in 10% SDS-PAGE for autoradiography to detect *in vivo* ADP-ribosylated SZF1/SZF2 proteins. Input proteins were detected by immunoblot with α-FLAG antibodies.

For *in vivo* macrodomain affinity resin- or PARP14m3 resin-mediated ADP-ribosylation assays, 1 mL of protoplasts expressing indicated constructs were treated with 0.1 μM flg22 for 1 hr. Total protein extracts were lysed in IP buffer and subjected for immunoprecipitation with macrodomain affinity resin (Tulip Biolabs, Inc.) or PARP14m3 magnetic affinity resin (Tulip Biolabs, Inc.). The immunoprecipitated proteins were detected by immunoblotting with the indicated antibodies.

For *in vitro* plant extract-mediated ADP-ribosylation assays, plant extracts were isolated from 0.03 g *Arabidopsis* leaves lysed in 100 μL lysis buffer (50 mM Tris-HCl, pH8.0, 50 mM NaCl, 1mM DTT, 10% Glycerol, 0.25% Triton X-100). Two μg of purified GST-SZF1, GST-SZF2, or GST-MBP (control) proteins were pre-incubated with glutathione agarose beads in 300 μL GST buffer for 1 hr at 4°C. The immobilized protein beads were washed twice with washing buffer and then incubated with plant extracts in a 20 μL ADP-ribosylation reaction buffer [50 mM Tris-HCl, pH8.0, 50 mM NaCl, 0.2 μM biotinylated NAD$^+$ (R&D system) or 1 μCi ^{32}P-NAD$^+$ (Perkin Elmer)] for another 1 hr. After reactions, the beads were collected and washed three times with a washing buffer to obtain the ADP-ribosylated SZF1 and SZF2 proteins. To detect the effect of PARG1, HsMacroD2, and HsPARG, two μg of indicated proteins were co-incubated with ADP-ribosylated SZF1 proteins derived from the above reaction in the reaction buffer (50 mM Tris-HCl, pH8.0, 50 mM NaCl) at 23°C for 3 hr. The reactions were stopped by adding 4x SDS loading buffer, and ADP-ribosylated proteins were separated in 10% SDS-PAGE and detected by streptavidin-HRP (Thermo Scientific) for biotinylated NAD$^+$ or visualized by ^{32}P-NAD$^+$ autoradiography.

Subcellular localization and FRET-FLIM assay

The fluorescence signals of GFP and mCherry fusion proteins were observed using a Leica TCS SP8 confocal laser scanning microscope (Germany). The excitation wavelength of GFP and mCherry is 488 nm and 588 nm, respectively. The emission wavelength for detecting GFP and mCherry is 490-530 and 590-620 nm, respectively. The autofluorescence of chloroplasts was excited at 630 nm, and the emission wavelength for detecting chloroplast signal is 690-700 nm. The pinhole was set at 1 Airy unit. Images and FLIM-FRET analyses were performed using Leica Application Suite X (LAS X) software as described (Bücherl et al., 2010). Briefly, FRET measurements were done with a pair of GFP/mCherry fusion proteins. The image of GFP donor fluorescence was analyzed and scanned at 488 nm and detected between 490 and 530 nm. The GFP fluorescence lifetime (τ) was calculated as the average of 10 (τ) values randomly measured in the protoplast cells for each pair of proteins analyzed. The Leica LAS X software measured the relative fluorescence intensity (I) in a specific region of interest (ROI) and lifetime (τ). FRET efficiency (E) was calculated by using the formula $E = 1-(\tau_{DA}/\tau_D)$, where τ_{DA} is the lifetime of the donor in the presence of acceptor and τ_D is the fluorescence lifetime of the donor alone. The statistical analysis was performed by one-way ANOVA for multiple comparisons.

Agrobacterium-mediated VIGS assay

The VIGS assay was performed as described previously (de Oliveira et al., 2016; Li et al., 2014). Briefly, the VIGS vectors *pTRV-RNA1* and *pTRV-RNA2* derivatives, *pYL156-SH3P1*, *pYL156-SH3P2*, *pYL156-PUB2*, *pYL156-MAC3A*, *pYL156-MAC3B*, or *pYL156-GFP* (the vector control) were introduced into *Agrobacterium tumefaciens* strain GV3101 by electroporation. Bacterial cultures were first grown in LB medium containing 50 μg/mL kanamycin and 25 μg/mL gentamicin overnight and then sub-cultured in fresh LB medium with the same antibiotics containing 10 mM MES and 20 mM acetosyringone for overnight at 28°C in a shaker with 180 rpm. Cells were harvested by ~2500 g centrifugation, re-suspended in the infiltration buffer (10 mM $MgCl_2$, 10 mM MES and 200 mM acetosyringone), adjusted to OD_{600} of 1.5, and incubated at 25°C for 3 hr. Bacterial cultures containing *pTRV-RNA1* and *pTRV-RNA2* derivatives were mixed at a 1:1 ratio and hand-infiltrated into the first pair of true leaves of two-week-old soil-grown plants using a needleless syringe.

ROS burst assay

True leaves of four-week-old soil-grown *Arabidopsis* plants for WT and different mutants were excised into leaf discs (5-mm diameter). Leaf discs were incubated with 100 μL ddH_2O in 96-well plates to eliminate the wounding effect. Leaf discs were soaked with a solution containing 50 μM luminol and 10 μg/mL horseradish peroxidase supplemented with 0.1 μM flg22. ROS burst was measured immediately after adding the solution by a luminometer (GloMax-Multi Detection System, Promega) for a period of ~35 min. The values for ROS production were indicated as means of relative light units (RLU).

RNA sequencing analysis

Ten-day-old seedlings of Col-0, *szf1,* and *szf2* mutants germinated on ½ MS agar plates were transferred to ddH_2O overnight and then treated with 0.1 μM flg22 or ddH_2O for 1 hr. The total RNA was extracted by the plant total RNA kit (MilliporeSigma). Three independent repeats were performed for RNA-Seq analysis using an Illumina HiSeq 2500 platform. Approximately 15 million reads

were obtained for each sample, which corresponds to ~30 x coverage of the *Arabidopsis* transcriptome. RNA-Seq reads with low sequencing quality or reads with sequencing adaptors were filtered by Trim_Galore version 0.6.5 [a wrapper of the Cutadapt program (Martin, 2011)]. The quality of the clean reads was then evaluated using FastQC version 0.11.9, and after passing quality control, the expression of the transcripts was quantified against the *Arabidopsis* reference transcriptome (TAIR10) using Salmon version 0.14.0 (Patro et al., 2017). These transcript abundances were then imported into R and summarized with tximport (Soneson et al., 2015), and then DESeq2 (Love et al., 2014) was used to normalize the raw counts and to perform differential expression analysis. Genes exhibiting fold change ≥ 2 or ≤ -2 and p value < 0.05 were classified as differentially expressed genes (DEG) between samples with or without flg22 treatment, which were used to generate the heatmap. GO term enrichment was analyzed using the latest *Arabidopsis* GO term annotations. The cutoff for significant enrichment is p value < 0.01 and q (false discovery rate) < 0.05. The fold enrichment was calculated based on the $-\log_{10}$(p value).

LC-MS/MS analysis

For MARylation site identification, 1 μg of GST-SZF1 or SZF2 was incubated with 1 μg of HIS-SRO2 in the ADP-ribosylation reaction buffer at 23°C for 6 hr. Meanwhile, 1 μg of GST-SZF1 or SZF2 was incubated with plant extracts in the reaction buffer at 23°C for 2 hr. NH_2OH (1 M) was added to the reactions to generate a hydroxamic acid derivative with an additional 15.0109 Da. The proteins were separated in 10% SDS-PAGE and stained with GelCode blue (Thermo Fisher). The SZF1 and SZF2 bands were sliced for LC-MS/MS analysis, as previously reported (Feng et al., 2016b) at the proteomics core of UT Southwestern Medical Center. Briefly, MARylated proteins were in-gel digested with trypsin overnight, and peptides were enriched for LC-MS/MS analysis with a Q-Exactive Plus Orbitrap mass spectrometer (Thermo Scientific). The MS/MS spectrum was analyzed using MaxQuant software with the default parameters. ADP-ribosylation at glutamate or aspartate residues with the addition of 15.0109 Da was manually inspected to ensure confident site detection.

For SZF1-associated protein identification, 10 g of *pSZF1::SZF1-FLAG/szf1* seedlings were ground into powder in a mortar containing liquid nitrogen, and the powder was lysed in the Co-IP buffer by vortexing. Protein extracts were incubated with α-FLAG agarose beads (MilliporeSigma) for 3 hr at 4°C with gentle shaking on a rocker. The beads were collected and washed three to five times with washing buffer, and the SZF1 complexes were eluted by elution buffer (0.2 M glycine, pH 2.5). The elution fraction was immediately neutralized by neutralization buffer (1 M Tris, pH 10.4) and was digested by trypsin to generate the peptides for LC-MS/MS analysis. The MS/MS spectrum was analyzed using MaxQuant software with the default parameters. The identified peptides were searched against the *Arabidopsis* protein database (TAIR11) to obtain detailed protein information.

QUANTIFICATION AND STATISTICAL ANALYSIS

Data for quantification analyses are presented as mean ± standard deviation (SD). The statistical analyses were performed by Student's t test or one-way analysis of variance (ANOVA) test (* $p < 0.05$, ** $p < 0.01$, *** $p < 0.001$; ****$p < 0.0001$; ns, no significant, $p \geq 0.05$) using the GraphPad Prism 8.0 software. The protein levels in the WB images were quantified by ImageJ software. The number of replicates is shown in the figure legends.